The Geological Society of America
Special Paper 555

Linking the Gulf of Mexico and Coast Mountains batholith during late Paleocene time: Insights from Hf isotopes in detrital zircons

Mark E. Pecha*
Department of Geosciences, University of Arizona, Tucson, Arizona 85721, USA

Michael D. Blum
Department of Geology, University of Kansas, Lindley Hall, 1475 Jayhawk Boulevard, Room 120, Lawrence, Kansas 66045, USA

George E. Gehrels
Department of Geosciences, University of Arizona, Tucson, Arizona 85721, USA

Kurt E. Sundell
Department of Geosciences, Idaho State University, Pocatello, Idaho 83209-8072, USA

Karl E. Karlstrom
Department of Earth and Planetary Sciences, University of New Mexico, Northrop Hall, Albuquerque, New Mexico 87131, USA

David A. Gonzales
Department of Geosciences, Fort Lewis College, 1000 Rim Drive, Durango, Colorado 81301, USA

David H. Malone
Department of Geography-Geology, Illinois State University, Normal, Illinois 61790, USA

J. Brian Mahoney
Department of Geology, University of Wisconsin–Eau Claire, 105 Garfield Avenue, Eau Claire, Wisconsin 54702, USA

ABSTRACT

Paleocene Lower Wilcox Group sedimentation rates are three times the Cenozoic average for the Gulf of Mexico region and are attributed to Laramide tectonism within the Laramide–Rocky Mountains region. These increased rates likely represent the erosion of easily weathered Phanerozoic strata that blanketed the Laramide-age basement-cored uplifts. Geologic observations and U-Pb geochronology are not sufficient to fully address this hypothesis alone, so we conducted 439 Lu-Hf isotopic

*Corresponding author: mpecha@email.arizona.edu

Pecha, M.E., Blum, M.D., Gehrels, G.E., Sundell, K.E., Karlstrom, K.E., Gonzales, D.A., Malone, D.H., and Mahoney, J.B., 2022, Linking the Gulf of Mexico and Coast Mountains batholith during late Paleocene time: Insights from Hf isotopes in detrital zircons, *in* Craddock, J.P., Malone, D.H., Foreman, B.Z., and Konstantinou, A., eds., Tectonic Evolution of the Sevier-Laramide Hinterland, Thrust Belt, and Foreland, and Postorogenic Slab Rollback (180–20 Ma): Geological Society of America Special Paper 555, p. 265–292, https://doi.org/10.1130/2021.2555(10).

analyses on detrital zircons from eight samples from the San Juan Basin and five samples from the Gulf of Mexico Basin. Focusing on the zircons younger than 300 Ma allowed us to make direct comparisons to the eight principal components that comprise the North American Cordilleran magmatic arc: (1) Coast Mountains batholith; (2) North Cascades Range; (3) Idaho batholith; (4) Sierra Nevada batholith; (5) Laramide porphyry copper province; (6) Transverse Ranges; (7) Peninsular Ranges; and (8) Sierra Madre Occidental. The $\varepsilon Hf_{(t)}$ results range from +8.9 to –27.0 for the San Juan Basin samples and from +13.0 to –26.6 for the Gulf of Mexico samples. Using the San Juan Basin samples as a proxy for the eroded Mesozoic cover that was shed from the Laramide uplifts, we show that much of the sediment entering the Gulf of Mexico through the Houston and Mississippi embayments during the late Paleocene was derived from reworked cover from the greater Laramide–Rocky Mountains region. However, the Gulf of Mexico samples also include a distinct juvenile suite ($\varepsilon Hf_{[t]}$ ranging from +13 to +5) of zircons ranging in age from ca. 220 to 55 Ma that we traced to the Coast Mountains batholith in British Columbia, Canada. This transcontinental connection indicates an extension to the headwaters of the previously defined paleo-Mississippi drainage basin from ca. 58 to 56 Ma. Therefore, we propose a through-going fluvial system (referred to here as the "Coast Mountains River") that was routed from the Coast Mountains batholith to the Gulf of Mexico. This expands the previously defined paleo-Mississippi drainage basin area by an estimated 280,000 km^2. Our comprehensive Hf isotopic compilation of the North American Cordilleran magmatic arc also provides a benchmark $\varepsilon Hf_{(t)}$ versus U-Pb age plot, which can be used to determine provenance of detrital zircons (85–50 Ma) at the scale of specific region(s) within the Cordillera based on their $\varepsilon Hf_{(t)}$ values.

INTRODUCTION

The Gulf of Mexico Basin is one of the largest sediment repositories on Earth, and since its inception in Middle Jurassic time, it has been filling with sediment from the North American craton (Galloway et al., 2011; Ewing and Galloway, 2019). Throughout most of the Mesozoic, clastic sediment supply rates to the Gulf of Mexico were relatively low due to high global sea levels, which allowed sediment derived from the Sevier and Laramide highlands to the west to accumulate within the Western Interior Seaway (Galloway et al., 2011), which occupied a continental-scale foreland basin (e.g., Miall et al., 2008), or due to rivers that flowed generally northeastward (e.g., Galloway et al., 2011; May et al., 2013; Loope and Secord, 2017; Wroblewski and Dunn, 2019), thus shielding the Gulf of Mexico. During late Paleocene time, sediment flux to the Gulf of Mexico region increased dramatically, and this is thought to have been the manifestation of changes in Laramide tectonism upstream (Galloway et al., 2011; Mackey et al., 2012; Blum and Pecha, 2014; Blum et al., 2017; Sharman et al., 2017). Climate change, drainage basin evolution, and intraplate tectonism all likely had an effect on sediment supply to the Gulf of Mexico Basin margin (Dickinson et al., 1988; Wilf, 2000; Sewall and Sloan, 2006; Lawton, 2008; Davis et al., 2009; Galloway et al., 2011; Mackey et al., 2012; Sharman et al., 2017; Smith et al., 2020). Drainage capture of ~900,000 km^2 within the Sevier-Laramide structural province, including the California (Davis et al., 2010) and Idaho Rivers (Chetel et al., 2011), has been proposed as the catalyst for this increase in sediment flux (Sharman et al., 2017). Regardless of the exact mechanism(s), it is certain that Laramide basement-cored uplifts, including their overlying Phanerozoic strata, contributed voluminous sediment to the Gulf of Mexico Basin. This notion provides the basic underpinnings for this study, the foundation of which we put to test by collecting Hf isotopic data from detrital zircons in the San Juan and Gulf of Mexico Basins.

Over the past ~10 yr, numerous U-Pb detrital zircon studies have been conducted on Gulf of Mexico strata (Galloway et al., 2011; Mackey et al., 2012; Blum and Pecha, 2014; Wahl et al., 2016; Sharman et al., 2017; Blum et al., 2017), as well as intraforeland basins in the Sevier-Laramide foreland of western North America (e.g., Davis et al., 2010; Lawton and Bradford, 2011; Dickinson et al., 2012; Laskowski et al., 2013; Donahue, 2016; Bush et al., 2016; Malone et al., 2017; Pecha et al., 2018; Smith et al., 2020; Anderson et al., 2019; Welch et al., this volume; Malone et al., this volume). These detrital zircon studies provide important contributions to the overall understanding of these depositional systems and insights into their potential provenance ties. Most of these studies, however, only employed U-Pb age data and geologic observations to make provenance interpretations. Acquiring Hf isotopic measurements on the detrital zircons allows for a more robust provenance interpretation by providing an additional data set for characterization of sediment source regions (e.g., Gehrels and Pecha, 2014; Sauer et al., 2017).

The power of Hf isotope geochemistry in detrital zircon provenance studies has been exhibited throughout the North American Cordillera (Gehrels and Pecha, 2014; Surpless et al.,

2014; Yokelson et al., 2015; Giesler et al., 2016; Pecha et al., 2016, 2018; White et al., 2016; Sauer et al., 2017; Surpless and Gulliver, 2018). In addition to crustal evolution information, Hf isotope measurements in zircon provide an additional diagnostic tool for detrital zircon provenance evaluation (Gehrels and Pecha, 2014); however, this also requires knowledge of the U-Pb age and Hf isotopic signature(s) of the potential source terranes. Fortunately, the principal magmatic provinces that constitute the North American Cordillera (i.e., Coast Mountains batholith, North Cascades Range, Idaho batholith, Sierra Nevada batholith, Peninsular Ranges batholith, Transverse Ranges, Sierra Madre Occidental, and Laramide porphyry copper province) are characterized in terms of their zircon Hf isotopic signature to a degree that is sufficient to provide a robust reference data set for comparisons with newly generated detrital Hf results (Arvizu and Iriondo, 2011; Cecil et al., 2011; Gaschnig et al., 2011; Lackey et al., 2012; Shaw et al., 2014; Barth et al., 2016; Mahar et al., 2016; Fisher et al., 2017; Homan, 2017; Sauer et al., 2017; Chapman et al., 2018; Dafov et al., 2020; Garcia et al., 2021).

Comparison of our new Hf data from the San Juan and Gulf of Mexico Basins with the principal tectonic/magmatic elements that constitute the North American Cordillera revealed provenance ties that improve our understanding of paleodrainage patterns and scales. Our data suggest that one or more continental-scale river(s) extended beyond previously defined catchments to include remote sources located in the Pacific Northwest, including the Coast Mountains batholith, British Columbia, Canada. The manner in which provenance was evaluated was fourfold: (1) Establish the detrital zircon epsilon Hf values of both the San Juan Basin and Gulf of Mexico Basin strata, (2) examine published Paleocene geologic and paleogeographic maps of the region, (3) compile and compare all the previously published Hf isotopic data on igneous zircons from the principal tectonic elements that make up the North American Cordillera, and (4) refine the paleodrainage patterns and catchment geometries during late Paleocene time. The results yielded important information into the genetic connection between the Laramide intraforeland uplifts and basins of the U.S. Rocky Mountains region and provided insights into continental-scale drainage networks and sediment pathways to the Gulf of Mexico. Our findings also provided insight into the crustal evolution of the North American Cordilleran magmatic arc, and allowed the development of a Laramide (ca. 85–50 Ma) detrital zircon epsilon Hf signature map, which can be used to refine provenance of zircons within this age range in and around western North America.

GEOLOGIC BACKGROUND

Sedimentary basins (e.g., San Juan Basin, Gulf of Mexico Basin) that form downstream from regional tectonic elements (e.g., Idaho batholith, Coast Mountains batholith, Sevier thrust belt, etc.) function as immense data repositories that can be accessed for research in a multitude of ways to better understand the upstream tectonic element(s). Basins peripheral to ancient orogenic systems often contain a comprehensive rock record that may provide geologic insight into the original orogenic system, even if large percentages of the original tectonic element(s) have been partially or completely removed by erosion (Gehrels and Pecha, 2014). Paired U-Pb and Hf detrital zircon provenance studies provide critical information that can be related back to the magmatic origin of the zircons, sediment provenance, maximum depositional age of the sediment, paleogeography, and landscape evolution.

Here, we summarize the geologic background of western North America during Mesozoic and early Cenozoic time, including the Cordilleran magmatic arc, Cordilleran foreland basin, San Juan intraforeland basin, and Gulf of Mexico Basin.

North American Cordilleran Magmatic Arc

Cordilleran-style magmatism in western North America initiated ca. 284 Ma in what is now central Mexico (Dickinson, 2004). The arc within this region was built on the edge of Gondwanan crust as the hypothetical Mezcalera plate subducted eastward beneath the southwestern edge of Laurentia (Dickinson and Lawton, 2001a; Dickinson, 2004). Permian through Early Triassic magmatism in southwestern Laurentia was limited to this region; however, by ca. 245 Ma, the Cordilleran magmatic arc was an established component of the circum-Pacific orogenic belt (Dickinson, 2000, 2004). This included initiation of subduction and subsequent magmatism within the Klamath-Sierran, Peninsular Ranges, and Coast Mountains batholith regions (Dickinson, 2000).

The Laurentian continental margin during mid-Mesozoic time consisted of an arc-trench system that experienced episodes of tectonic accretion of intra-oceanic island-arc systems (Dickinson, 2004). This accretionary stage was followed by emplacement of a belt of batholiths along the majority of the Cordillera from Late Jurassic and through Cretaceous time. Today, the principal record of Cordilleran arc magmatism is this group of Cretaceous batholiths, which extend discontinuously along the entire Cordilleran margin from Mexico to southeastern Alaska. These batholiths often have unique isotopic signatures, offering potential isotopically distinct sources of detrital zircons preserved in basins downstream. Due to spatial variations in basement geology, the batholiths typically have isotopic characteristics specific to their geographical region.

Cordilleran Foreland Basin and Laramide Intraforeland Basins

During late Mesozoic time, the U.S. Rocky Mountain region was part of an expansive Cordilleran foreland basin system that formed due to flexural subsidence caused by loading from the Sevier thrust belt (Fig. 1; Armstrong, 1968; Jordan, 1981; DeCelles, 2004; Craddock et al., this volume). The foreland basin was flanked on the west by the Sevier thrust belt, including the high-elevation Nevadaplano plateau (DeCelles,

2004), and on the southwest by the Mogollon Highlands rift shoulder, a high-standing structural feature related to the formation of the Bisbee-McCoy basin (Dickinson and Lawton, 2001b; Lawton, 2004; Lucas, 2004; Dickinson and Gehrels, 2008). Beginning in Late Cretaceous (ca. 85 Ma) time, Laramide deformation and magmatism partitioned the once-continuous Sevier foreland basin into isolated intraforeland basins and intervening basement block uplifts (Lowell, 1974; Bird, 1984; Brown, 1988; Dickinson et al., 1988; Cather, 2004; DeCelles, 2004; Carrapa et al., 2019; Lawton, 2019; Craddock et al., this volume). The most popular explanation for the inland migration of Laramide deformation and magmatism is flat-slab subduction of the Farallon plate beneath the western edge of Laurentia (e.g., Coney and Reynolds, 1977; Dickinson and Snyder, 1978; Miller et al., 1992; English et al., 2003; Saleeby 2003; Liu et al., 2010). Within the southern Rocky Mountains region, the manifestations of Laramide deformation include basement-cored uplifts bounded by high-angle reverse faults (e.g., Nacimiento uplift)

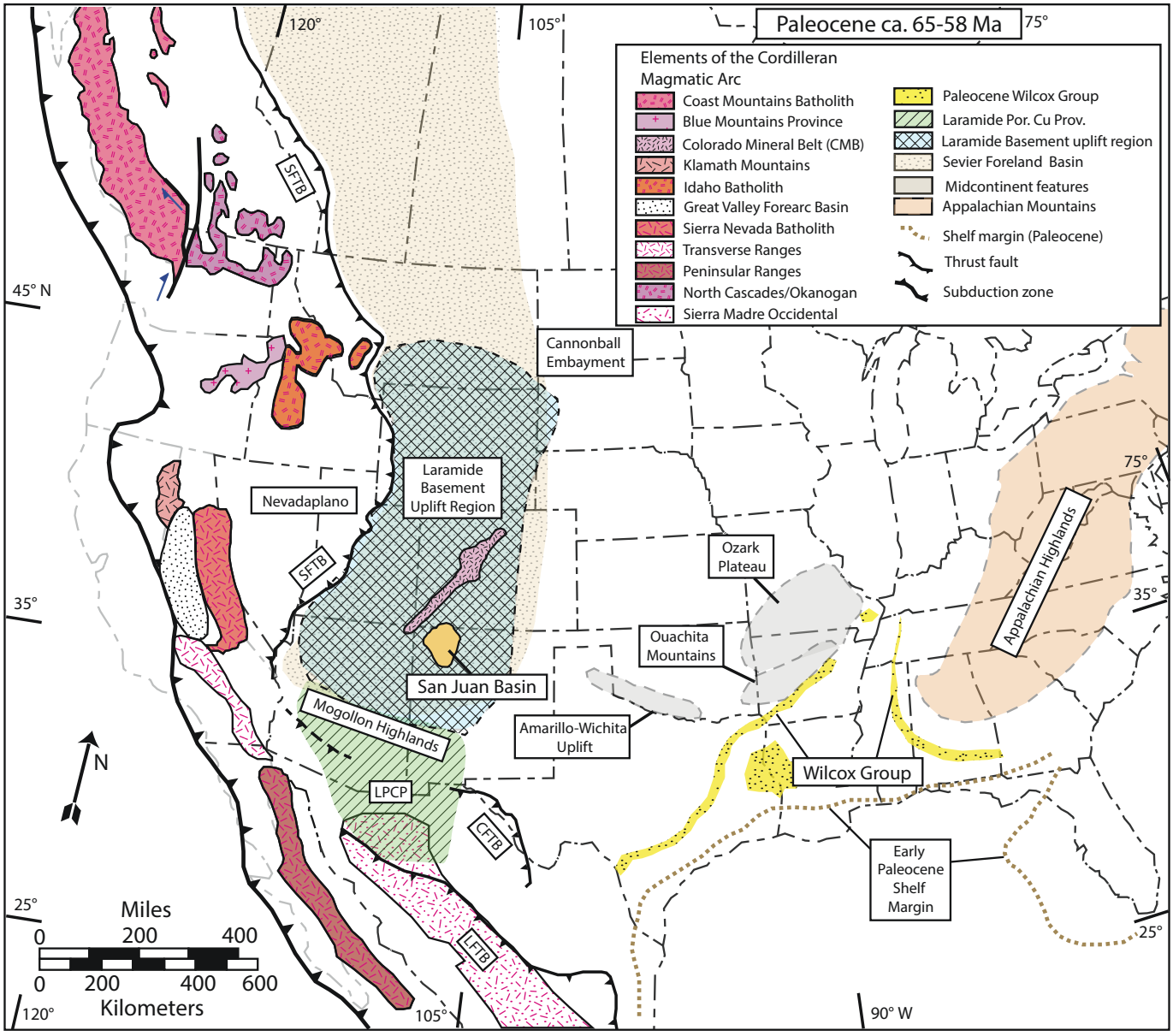

Figure 1. Generalized tectonic map of North America showing the spatial relationship between the San Juan Basin, Gulf of Mexico, and the major tectonic elements of the North American Cordillera. Tectonic elements within the North American Cordilleran arc are indicated as follows: SFTB—Sevier fold-and-thrust belt, Nevadaplano (DeCelles, 2004); LPCP—Laramide porphyry copper (Por. Cu) province (Leveille and Stegen, 2012); LFTB—Laramide fold-and-thrust belt; CFTB—Chihuahua-Coahuila fold-and-thrust belt. Figure is based on Galloway et al. (2011), Blum and Pecha (2014), Blum et al. (2017), and restored palinspastically after Dickinson et al. (2012); Coast Mountains batholith restoration is after Wyld et al. (2006). K—Cretaceous; J—Jurassic.

or broad monoclines (e.g., Monument uplift), where the high-angle reverse faults may or may not penetrate the surficial geology. Twenty-three distinct Laramide intraforeland basins exist within the Rocky Mountains region, each preserving variable thicknesses of Cretaceous through Eocene strata (Cather, 2004; Galloway et al., 2011; Lawton, 2019).

Laramide uplift and erosion played important roles in the formation of the geomorphology of the Four Corners region (Utah–Colorado–Arizona–New Mexico; Elston and Young, 1991; Cather, 2004; Cather et al., 2012). Estimates for the thickness of Triassic and Jurassic strata that has been removed by erosion from the Colorado Plateau region range from ~1000 to 1500 m (Pederson et al., 2002; Lazear et al., 2013). This is in addition to the estimated ~300–1000 m of Cretaceous strata that were removed during Cenozoic beveling (Epis and Chapin, 1975; Pazzaglia and Kelley, 1998). This pervasive erosion has resulted in the removal of many Cretaceous and younger rocks on the Colorado Plateau, but the San Juan Basin is an exception, preserving a sequence of Cretaceous and early Paleogene rocks exceeding 2000 m in total thickness.

San Juan Basin

The San Juan Basin in northwestern New Mexico and southwestern Colorado is a structurally controlled intraforeland Laramide basin. The basin developed coeval with the surrounding Laramide uplifts (Defiance uplift, Hogback monocline, San Juan uplift, Archuleta anticlinorium, Nacimiento uplift, Zuni uplift, and the Colorado Mineral belt; Fig. 2), as evidenced by Late Cretaceous and Paleogene growth strata (ca. 80–50 Ma) along the western margin of the basin adjacent to the Nacimiento thrust (Kelley, 1950, 1951; Baltz, 1967; Molenaar, 1983). Attenuated

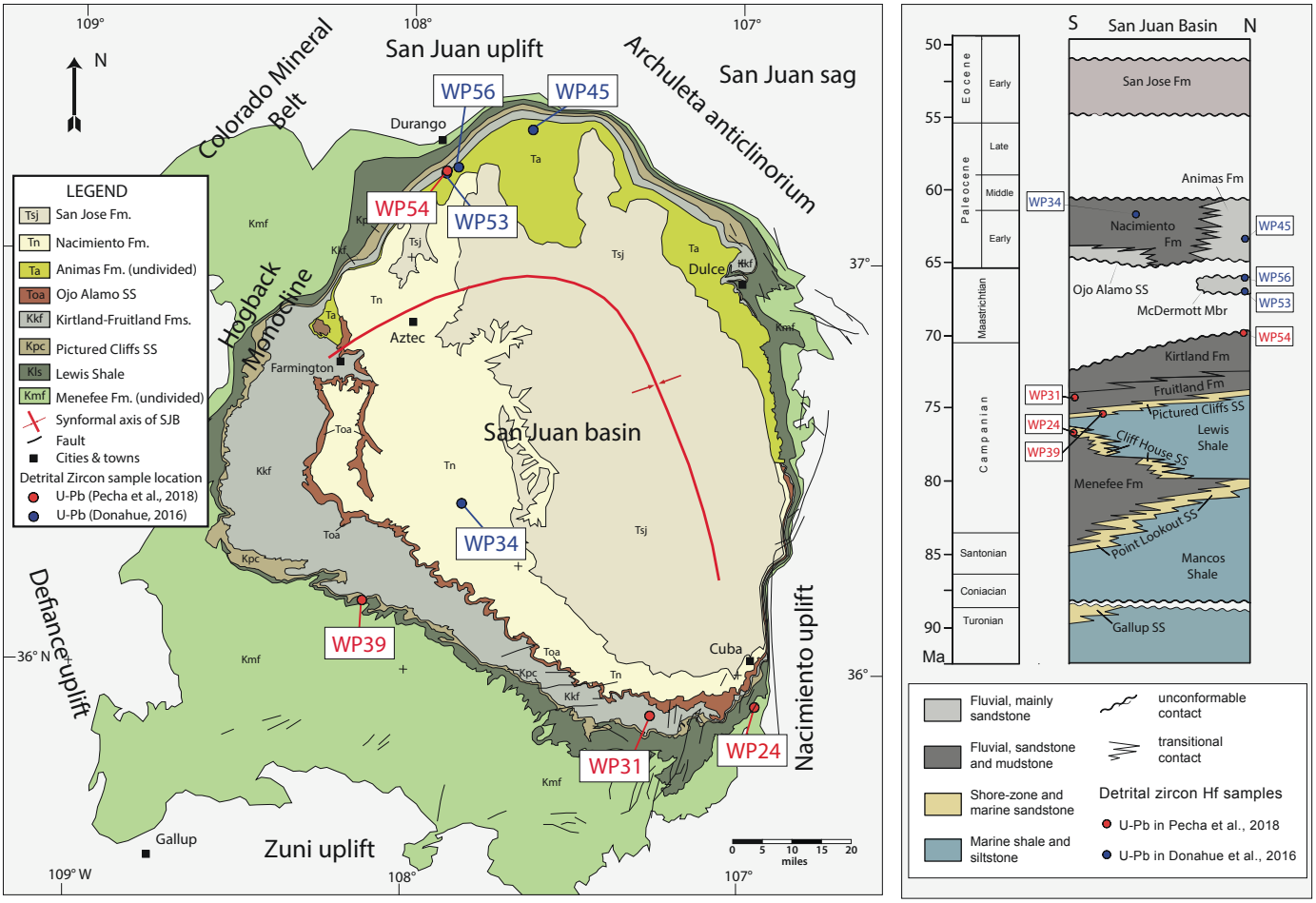

Figure 2. Simplified geologic map and stratigraphic column of the San Juan Basin (SJB), northwestern New Mexico and southwestern Colorado. Surrounding Laramide features are indicated in bold print: Colorado Mineral Belt, San Juan uplift, San Juan sag (Brister and Chapin, 1994), Archuleta anticlinorium, Nacimiento uplift, Zuni uplift, Defiance uplift, Hogback monocline. Detrital zircon U-Pb and Hf samples are indicated with sample number (e.g., WP56) and color-coded by reference: red (Pecha et al., 2018) and blue (Donahue, 2016). Base geologic map is modified from the *Geologic Map of New Mexico* (New Mexico Bureau of Geology and Mineral Resources, 2003, scale 1:500,000). Schematic stratigraphic column of Cretaceous (Late Turonian) through Eocene strata of the San Juan Basin is modified from Cather (2003, 2004). Geologic time scale is based on Walker and Geissman (2009). SS—Sandstone.

and steeply dipping units also occur along the northern margin of the basin. Beginning in Campanian time (ca. 75 Ma), flexural subsidence within the interior basin caused differential subsidence and sedimentation, resulting in an asymmetrical synform with an arcuate axial trace that mimics the trend of the bounding features on the west and north sides of the basin (Ayers et al., 1994; Cather, 2003, 2004; Cather et al., 2019).

The San Juan Basin contains the most complete section of Upper Cretaceous and Paleogene stratigraphy within the central Sevier-Laramide foreland. Upper Cretaceous strata were deposited during basinwide transgressive and regressive cycles associated with excursions of the Western Interior Seaway (Fassett and Hinds, 1971). During this time, rivers flowed from highlands located to the south and west and fed deltaic systems along the western margin of the Western Interior Seaway. By Paleocene time, Laramide deformation had significantly altered the regional drainage patterns, including creation of a subregional drainage divide along the axis of the Colorado Mineral Belt (Cather et al., 2012). Paleogene strata within the San Juan Basin are composed of fluvial and lacustrine deposits. Detailed sedimentologic descriptions of the Upper Cretaceous and Paleogene units are available in Craigg (2001).

Cretaceous and Paleocene fluvial and lacustrine deposits within the San Juan Basin and other Laramide intraforeland basins indicate that the majority of the Laramide province was likely above sea level throughout the entirety of the Laramide orogeny (Dickinson et al., 1988). During Paleocene time, most of the intraforeland perimeter basins north of the San Juan Basin were drained by fluvial systems that flowed toward the east, toward remnants of the Cretaceous interior seaway (Dickinson et al., 1988). Paleocene exit rivers from the San Juan Basin and other Laramide basins in New Mexico and Colorado (e.g., El Rito–Galesteo, Baca, etc.) existed and likely continued southeastward toward Gulf of Mexico depocenters (Gorham and Ingersoll, 1979; Klute, 1986; Dickinson et al., 1988; Cather, 2004; Galloway et al., 2011; Lawton, 2019). The final retreat of the Western Interior Seaway, including the Cannonball Sea, was complete by ca. 58 Ma, allowing for fluvial transport of sediments across the Great Plains (Slattery et al., 2015, and references therein). Comparisons between Cretaceous and Paleocene sedimentary rocks in the San Juan Basin and Gulf of Mexico Basin are essential in establishing first-order upstream/downstream connections. However, it is important to note that there is no direct correlation between rocks of the San Juan Basin and rocks of the Gulf of Mexico Basin, but rather that the rocks of the San Juan Basin provide a proxy for the rocks that once existed throughout the greater Four Corners region and likely throughout much of the Laramide province.

The out-of-phase nature of episodic sedimentation between the Laramide intraforeland basins and the Gulf of Mexico Basin has been well documented and certainly holds important implications for understanding their relationship (Cather, 2004; Sharman et al., 2017; Cather et al., 2019; Smith et al., 2020). Three rapid pulses of sedimentation occurred in the San Juan Basin at distinct intervals throughout Laramide time, each of which is separated by condensed sand-rich units (e.g., Kimbeto Member of the Ojo Alamo Sandstone) that accumulated during episodes of basin overfilling (Cather, 2004; Cather et al., 2019). The Paleocene upper Nacimiento Formation and the earliest Eocene Cuba Mesa Member of the San Jose Formation (including the lacuna of >5 m.y. that locally divides them) are the sand-rich condensed units found within the San Juan Basin that are approximately coeval with Wilcox Group sedimentation in the Gulf of Mexico (Cather, 2004; Cather et al., 2019).

Gulf of Mexico Basin

The geologic evolution of the Gulf of Mexico Basin is well understood due to the intense scrutiny of both academic and industry research conducted over the past ~80 yr. This includes studies on basin architecture, basin fill/stratigraphy, depositional environments, sediment dispersal patterns, and first-order paleogeography, summaries of which can be found in Galloway (2008), Galloway et al. (2011), Blum et al. (2017), and Ewing and Galloway (2019).

Oceanic seafloor spreading initiated during Middle Jurassic time, creating accommodation space within the Gulf of Mexico region, and continued evolving through Early Cretaceous time (Galloway et al., 2011). Gulf of Mexico drainage patterns transformed throughout late Mesozoic and Cenozoic time in response to hinterland tectonism in North America (Galloway, 2008; Galloway et al., 2011; Blum and Pecha, 2014), but in general, Gulf of Mexico sedimentation during the Paleocene was focused into three principal structural embayments (Fig. 3): (1) Rio Grande embayment, (2) Houston embayment, and (3) Mississippi embayment (Galloway et al., 2011; Mackey et al., 2012; Blum et al., 2017). Upper Paleocene to Lower Eocene Wilcox Group strata in east-central Texas were deposited within the Houston embayment. During Paleocene and early Eocene time, the Houston embayment drainage basin is thought to have encompassed the southern portion of the Sevier foreland, including the Four Corners region (Fig. 4; Galloway, 2008; Galloway et al., 2011; Blum and Pecha, 2014; Blum et al., 2017). Wilcox Group strata in central and southwestern Arkansas lie east of the Sabine uplift and were deposited within the Mississippi embayment, for which the drainage basin likely included the paleo-Mississippi, paleo-Arkansas, and paleo-Platte rivers. However, it is important to note there is ongoing debate regarding the specific sediment-routing pathways during this time frame, both within the hinterland and across the midcontinent region (Galloway et al., 2011; Mackey et al., 2012; Blum and Pecha, 2014; Wahl et al., 2016; Sharman et al., 2017; Blum et al., 2017; Lawton, 2019). The paleo-Platte and paleo-Arkansas rivers were draining western highlands, including the Nevadaplano and Idaho batholith regions (Sharman et al., 2017), while the paleo-Mississippi river was draining the midcontinent region and Appalachian sources to the east (Galloway et al., 2011; Blum and Pecha, 2014; Blum et al., 2017; Finzel, 2017; Sharman et al., 2017). All three of

these paleorivers were channeled through the paleo-Mississippi embayment en route to their destination in the Gulf of Mexico (Galloway, 2008; Galloway et al., 2011; Blum and Pecha, 2014; Blum et al., 2017).

Wilcox Group Sedimentation

Throughout the Mesozoic Era, clastic sediment supply rates to the Gulf of Mexico from the western continental interior (including the Sevier thrust belt and Laramide basement uplifts) were relatively low, primarily due to sediment sequestration within the Western Interior Seaway (Galloway et al., 2011). However, during deposition of the late Paleocene Lower Wilcox Group, sediment supply increased dramatically (to approximately three times the Cenozoic average), causing delta progradation, depositional offlap, and accumulation of sand-rich turbidite lobes on the Gulf of Mexico abyssal plain (Galloway et al., 2011; Zarra et al., 2019).

The links between the Laramide intraforeland basins and their associated basement-cored uplifts, and their downstream connection to sedimentation in the Gulf of Mexico Basin have been previously documented (Galloway et al., 2000, 2011; Galloway, 2005; Mackey et al., 2012; Sharman et al., 2017; Blum et al., 2017; Foreman et al., this volume). One possible link to the decrease in sediment supply to the Upper Wilcox Group relates to the unroofing of resistant basement cores of Laramide uplifts by earlier removal of the more easily eroded overlying Phanerozoic strata (Carroll et al., 2006). However, it is also probable that the formation of lacustrine environments due to hydraulic closure (e.g., Uinta Basin, Green River Basin) within the Laramide interior contributed to starve the system of sediment (Dickinson et al., 1988; Smith et al., 2014; Sharman et al., 2017), a notion that is supported by the out-of-sync sedimentation rates between many of the intraforeland basins and the Gulf of Mexico strata (Cather, 2004; Cather et al., 2019). Empirical data showing that mudstones and sandstones erode at a rate that is two to three orders of magnitude faster than granite or quartzite (Sklar and Dietrich, 2001) support the notion that unroofing of the basement cores likely played a role in starving the Gulf of Mexico during Upper Wilcox Group deposition. The stratigraphy of the Cordilleran foreland basin is regionally dominated by relatively soft and easily erodible Cretaceous sandstone and shale, resting on top of pre–foreland basin Triassic–Jurassic siliciclastic and evaporitic units. These strata rest on Upper to Lower Paleozoic, relatively resistant, carbonate-rich rocks, which in turn sit on top of Archean and Proterozoic basement rocks. The proportion of nonresistant to resistant rocks above the basement is roughly two-to-one, such that initial growth of Laramide basement-cored uplifts would have driven rapid erosion of the upper two thirds of the stratigraphic section, followed by somewhat slower dissection of the more resistant Paleozoic and, ultimately, Precambrian rocks (DeCelles et al., 1991; Carroll et al., 2006).

METHODS

To evaluate the genetic relationship between the San Juan and Gulf of Mexico Basins, we conducted Lu-Hf measurements

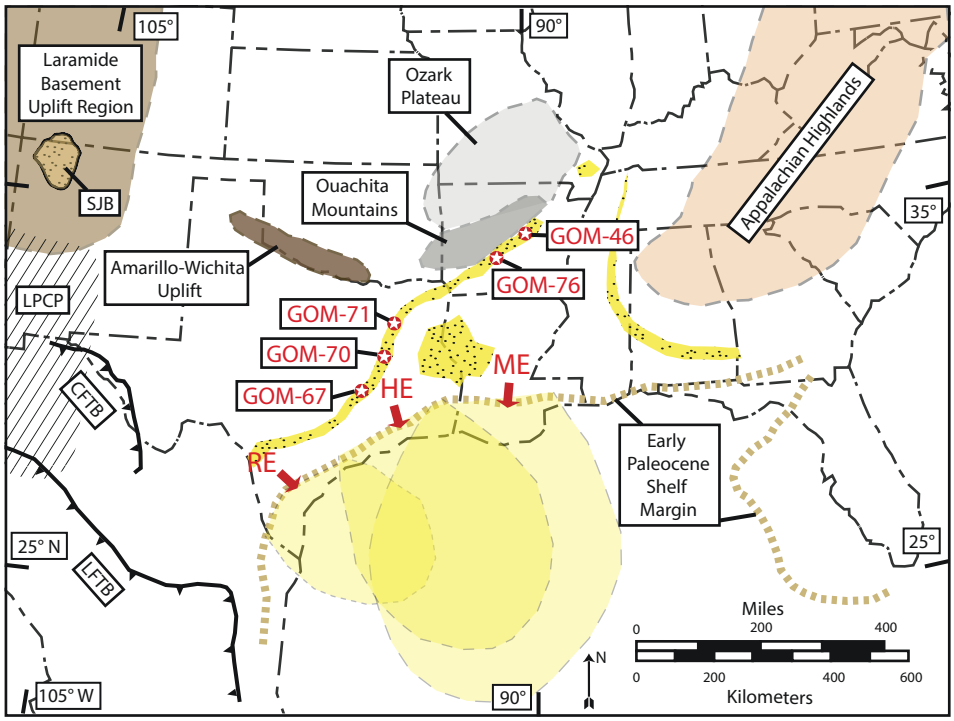

Figure 3. Outcrop map of the Paleocene Wilcox Group, Gulf of Mexico Basin. Hf samples designated by number correspond with U-Pb age dates from Blum and Pecha (2014). Gulf of Mexico structural embayments (after Galloway et al., 2011) are labeled: RE—Rio Grande embayment; HE—Houston embayment; ME—Mississippi embayment. Other abbreviations: LPCP—Laramide porphyry copper province (Leveille and Stegen, 2012); LFTB—Laramide fold-and-thrust belt; CFTB—Chihuahua-Coahuila fold-and-thrust belt; SJB—San Juan Basin. Base map and geology are based on Blum and Pecha (2014) and Blum et al. (2017).

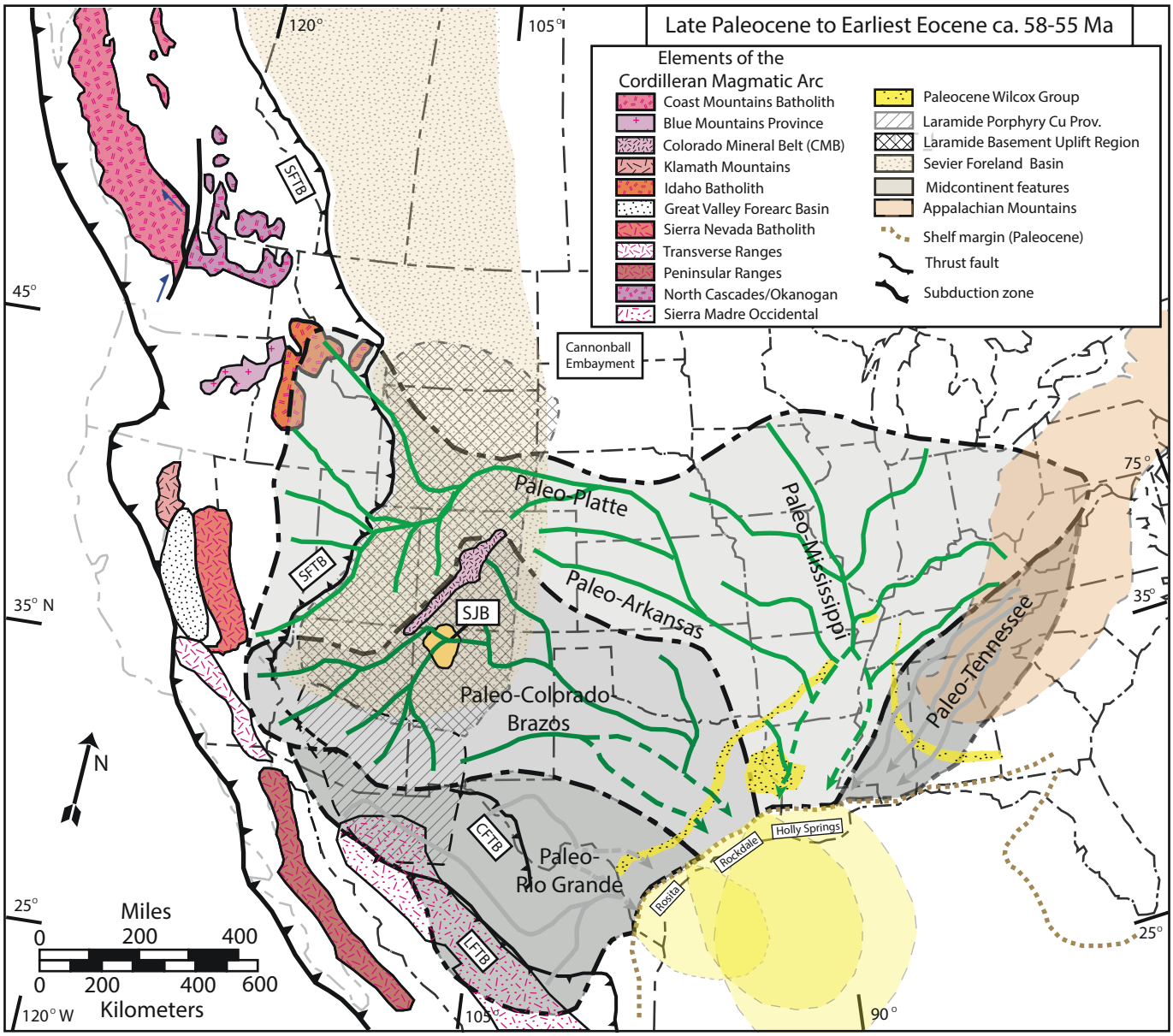

Figure 4. Paleodrainage reconstruction for the northern Gulf of Mexico during late Paleocene to early Eocene (ca. 58–55 Ma) time, after Blum et al. (2017), in relation to the major elements of the North American Cordillera. Rosita, Rockdale, and Holly Springs depocenters are after Fisher and McGowen (1969), Edwards (1981), and Galloway et al. (2011), and predicted slope and basin-floor fan are after Blum et al. (2017). Map illustrates the spatial relationships of these depositional systems with potential source regions located within the North American Cordillera as follows: SFTB—Sevier fold-and-thrust belt (DeCelles, 2004); LFTB—Laramide fold-and-thrust belt; CFTB—Chihuahua-Coahuila fold-and-thrust belt; SJB—San Juan Basin.

on all zircons with U-Pb ages younger than 300 Ma, dated by Donahue (2016; ~100 U-Pb analyses per sample); Pecha et al. (2018; ~100 U-Pb analyses per sample); Blum and Pecha (2014; ~100 U-Pb analyses per sample); Blum et al. (2017; ~300 U-Pb analyses per sample); and newly reported U-Pb ages here (~315 U-Pb analyses per sample) from 13 samples from the two basins (eight from San Juan Basin and five from the Wilcox Group in the Gulf of Mexico Basin; Figs. 2 and 3, respectively).

U-Th-Pb Geochronology

Four of the five zircon mounts from Blum and Pecha (2014) were unavailable for Lu-Hf analysis, so these samples (MDB-67, MDB-69, MDB-70, MDB-71) were remounted from a representative split of the original zircon yields and reanalyzed for U-Th-Pb. The nonmagnetic, heavy mineral fraction from each sample was incorporated into a 2.5 cm epoxy mount, sanded

~20 μm to expose the interior of each grain, and backscattered electron (BSE) imaged using a Hitachi S-3400N scanning electron microscope (SEM). The U-Th-Pb laser analyses were performed by laser ablation–inductively coupled plasma–mass spectrometry (LA-ICP-MS) using a Photon Machines G2 excimer laser connected to an Thermo Element 2 single-collector ICP-MS at the Arizona LaserChron Center (ALC) following established analytical protocols reported in Pullen et al. (2018). In total, 315 U-Pb laser analyses were completed on each detrital sample using a laser beam diameter of 20 μm. Complete analytical methodology, results, and maximum depositional age (MDA) analyses can be found in Supplemental File S1.[1]

Hf Isotopic Analysis

Hf isotope geochemistry of detrital zircons was conducted by laser ablation–multicollector–inductively coupled plasma–mass spectrometry (LA-MC-ICP-MS) at the Arizona LaserChron Center following established analytical protocols reported in Cecil et al. (2011) and Gehrels and Pecha (2014). On average, 35 Hf laser analyses were conducted per detrital sample. Analysis pit locations within each zircon were identified on high-resolution BSE images, and in all instances, the 40 μm Hf laser pits were placed directly on top of the earlier 20 μm U-Pb analysis pits, ensuring that all Hf laser analyses were located entirely within the same growth zone/domain as the earlier U-Pb pit. During each Hf data acquisition, we also monitored the down-hole $^{176}Hf/^{177}Hf$ to ensure we did not cross boundaries within any of the analyses. Comprehensive Hf isotopic data, including Hf evolution and epsilon Hf plots of individual samples, are presented in Supplemental File S2.

The newly acquired Hf data are presented in two-dimensional Hf-evolution diagrams (Figs. 5, 6, and 7C) and three-dimensional diagrams (Figs. 7A and 7B) that were generated using the Matlab graphical interface HafniumPlotter from Sundell et al. (2019), with bivariate kernel density estimates based on standard optimization parameters from Botev et al. (2010). The initial $^{176}Hf/^{177}Hf$ ratios are expressed in $\varepsilon Hf_{(t)}$ notation, which represents the Hf isotopic composition at the time of zircon crystallization relative to the chondritic uniform reservoir (CHUR; Bouvier et al., 2008). Internal precision for $^{176}Hf/^{177}Hf$ and $\varepsilon Hf_{(t)}$ is reported for each individual analysis on the final Hf data table in Supplemental File S1, and as the average of all unknown analyses (±1.4 epsilon units at 2σ) on Figures 5 and 6. Average external precision of ~1.33 epsilon units (2σ) was based on in-run analysis of six different zircon standards (R-33, Temora, Mud Tank, Plesovice, 91500, and FC1). Hf isotopic evolution of average (felsic) continental crust is shown with an arrow on all εHf evolution diagrams and is based on a $^{176}Lu/^{177}Hf$ ratio of 0.0115 (Vervoort and Patchett, 1996; Vervoort et al., 1999).

[1]Supplemental Material. Zircon U-Pb and Hf isotopic data. Please visit https://doi.org/10.1130/SPE.S.19184726 to access the supplemental material, and contact editing@geosociety.org with any questions.

The complete Lu-Hf analytical results are reported in Supplemental File S2, which also includes all previously reported Hf results that were used in our reference comparisons. All zircons analyzed for their Hf isotopic signatures were previously U-Pb age dated by LA-ICP-MS (Blum and Pecha, 2014; Donahue, 2016; Pecha et al., 2018; or newly reported here), and all new results are presented here in $\varepsilon Hf_{(t)}$ notation at 2σ, unless indicated otherwise. Table 1 is a summary of detrital zircon Hf data; Table 2 summarizes compiled Hf data for the Cordilleran magmatic arc.

U-Th-Pb GEOCHRONOLOGICAL RESULTS

Gulf of Mexico Samples

Sample MDB-67 produced 301 robust U-Pb laser analyses, of which 79 were Mesozoic or Cenozoic in age. The older part of the age spectra consists of scattered Archean ages from 2968 to 2537 Ma, Proterozoic ages ranging from 2498 to 574 Ma (age peaks 1774, 1701, 1448, 1190, 1112, and 1030 Ma), and scattered Paleozoic ages ranging from 536 to 280 Ma. The younger portion of the age spectra consists of Mesozoic ages ranging from 227 to 67.8 Ma (peak ages of 165, 96.0, and 75.4 Ma) and Cenozoic ages ranging from 65.8 to 60.6 Ma (peak age of 61.7 Ma). The MDA weighted average age consisting of the eight youngest analyses is 61.75 ± 0.54 Ma, with mean square of weighted deviates (MSWD) = 0.91.

Sample MDB-69 produced 288 robust U-Pb laser analyses, of which 95 were Mesozoic or Cenozoic in age. The older part of the age spectra consists of scattered Archean ages from 3270 to 2625 Ma, Proterozoic ages ranging from 2498 to 545 Ma (age peaks 1706, 1425, 1188, and 1087 Ma), and Paleozoic ages ranging from 535 to 257 Ma (peak age 259 Ma). The younger portion of the age spectra consists of Mesozoic ages ranging from 244 to 66.1 Ma (peak ages of 179, 165, 93.6, 73.1, and 66.2 Ma) and Cenozoic ages ranging from 65.0 to 60.1 Ma (peak ages of 63.1 and 61.1 Ma). The MDA weighted average age consisting of the nine youngest analyses is 61.52 ± 0.59 Ma, with MSWD = 1.01.

Sample MDB-70 produced 291 robust U-Pb laser analyses, of which 85 were Mesozoic or Cenozoic in age. The older part of the age spectra consists of Archean ages from 2876 to 2540 Ma (peak age of 2703), Proterozoic ages ranging from 2492 to 541 Ma (age peaks 1703, 1431, and 1095 Ma), and scattered Paleozoic ages ranging from 534 to 258 Ma. The younger portion of the age spectra consists of Mesozoic ages ranging from 224 to 67.5 Ma (peak ages of 170, 161, 113, 96.0, 75.5, 72.7, and 68.0 Ma) and Cenozoic ages ranging from 61.1 to 57.2 Ma (peak ages of 60.2 and 58.2 Ma). The MDA weighted average age consisting of the five youngest analyses is 58.65 ± 0.63 Ma, with MSWD = 1.6.

Sample MDB-71 produced 298 robust U-Pb laser analyses, of which 132 were Mesozoic or Cenozoic in age. The older part of the age spectra consists of scattered Archean ages from 2735 to 2537 Ma, Proterozoic ages ranging from 2484 to 556 Ma (age

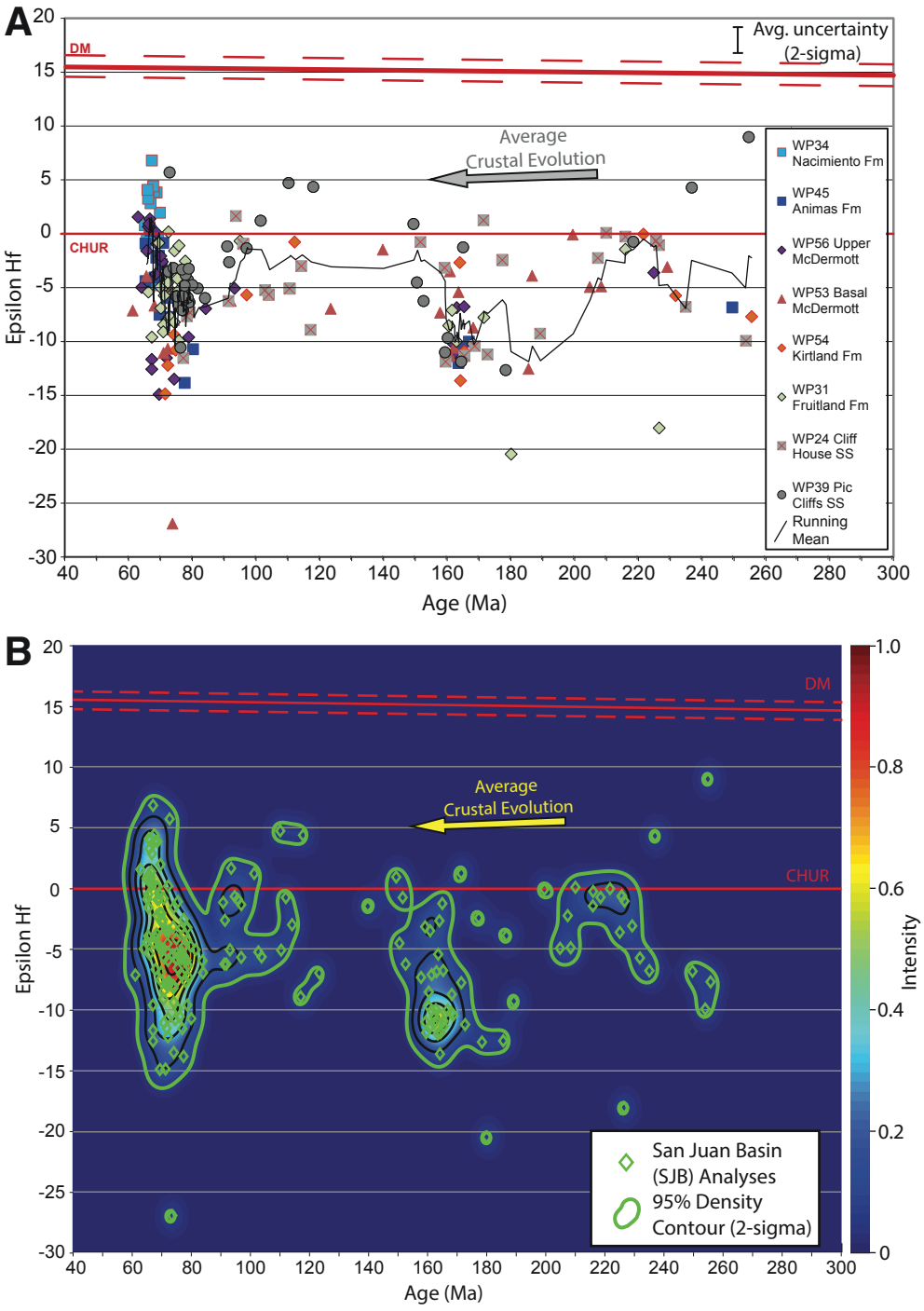

Figure 5. Hf isotopic data for San Juan Basin samples. (A) Epsilon Hf vs. U-Pb age plot of individual zircon analyses, which are color coded by sample. Black line is running average based on bin width of five analyses. DM—depleted mantle reservoir reference from Vervoort and Blichert-Toft (1999); CHUR—chondritic uniform reservoir from Bouvier et al. (2008); SS—Sandstone. (B) Two-dimensional density plot of epsilon Hf vs. U-Pb age of all San Juan Basin analyses. Green lines are 95% confidence contour interval. Density plot was generated using HafniumPlotter (Matlab script) from Sundell et al. (2019). Average crustal evolution arrows are based on $^{176}Lu/^{177}Hf$ ratio of 0.0115 (Vervoort and Patchett, 1996; Vervoort et al., 1999; Amelin et al., 1999, 2000).

peaks 1694, 1438, 1198, and 1053 Ma), and scattered Paleozoic ages ranging from 504 to 253 Ma. The younger portion of the age spectra consists of Mesozoic ages ranging from 251 to 66.2 Ma (peak ages of 162, 101, 92.4, 89.6, 72.7, and 68.0 Ma) and Cenozoic ages ranging from 65.4 to 47.2 Ma (peak ages of 58.9 and 56.8 Ma). The MDA weighted average age consisting of four ages (note: the youngest three analyses were excluded because of excessive scatter) is 56.36 ± 0.60 Ma, with MSWD = 0.74.

Hf ISOTOPE GEOCHEMISTRY RESULTS

San Juan Basin Samples

In total, 193 Lu-Hf laser analyses were conducted on eight detrital samples from across the San Juan Basin. This included 74 zircons ranging in age from 256 Ma to 102 Ma with $\varepsilon Hf_{(t)}$ ranging from +8.9 to –20.6, and 193 zircons ranging in age from 97 Ma

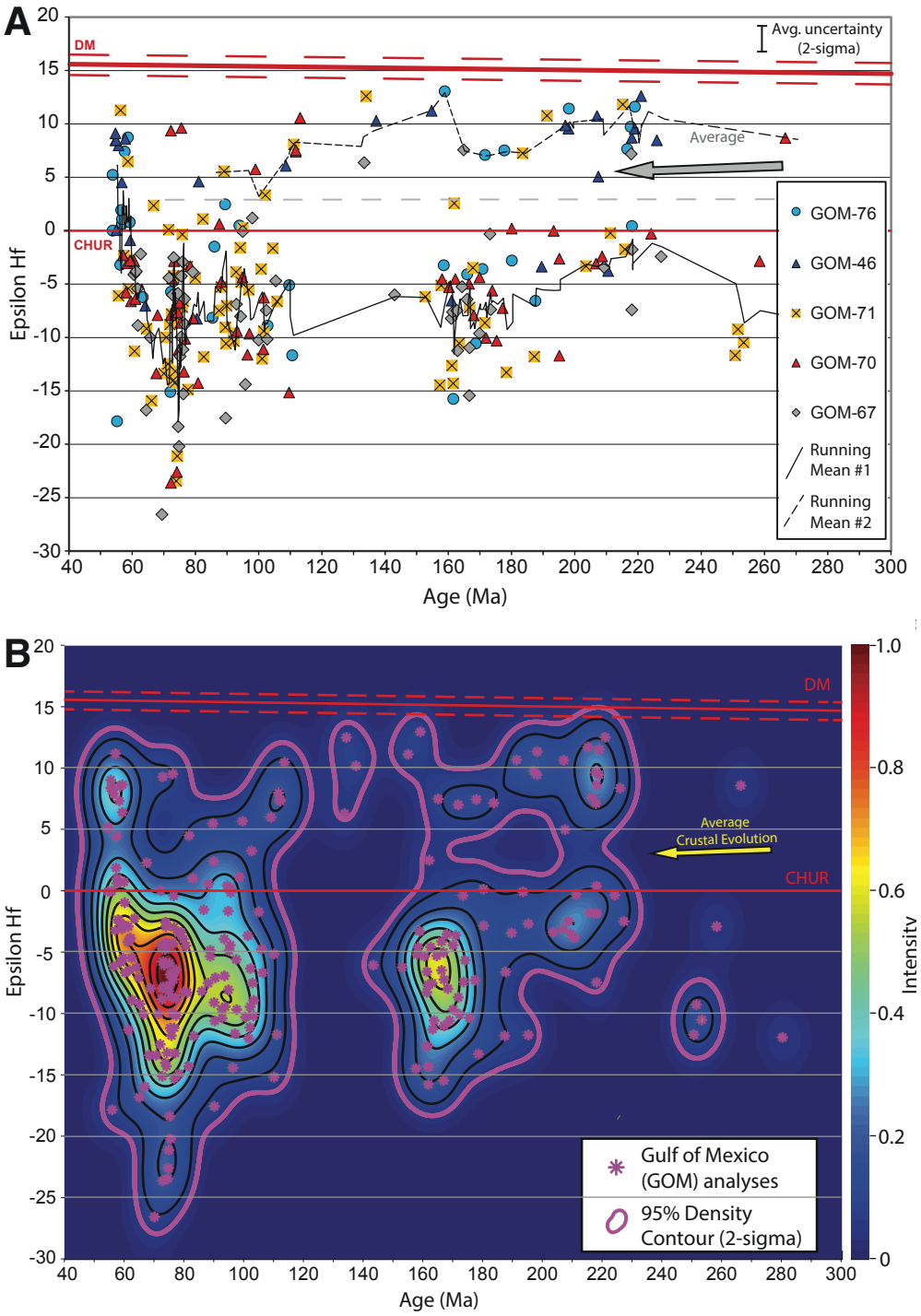

Figure 6. Hf isotopic data for Wilcox Group, Gulf of Mexico Basin samples. (A) Epsilon Hf vs. U-Pb age plot of individual zircon analyses, which are color coded by sample. Two distinct trends within the data are separated with the gray dashed line. Black lines are running averages based on bin width of five analyses; top running average only contains data from above the gray dashed line, and bottom running average only uses data from below the gray dashed line. DM—depleted mantle reservoir reference from Vervoort and Blichert-Toft (1999); CHUR—chondritic uniform reservoir from Bouvier et al. (2008). (B) Two-dimensional density plot of epsilon Hf vs. U-Pb age of all Wilcox Group, Gulf of Mexico analyses. Purple lines are 95% density contour intervals generated using HafniumPlotter (Matlab script) from Sundell et al. (2019). Average crustal evolution arrows are based on $^{176}Lu/^{177}Hf$ ratio of 0.0115 (Vervoort and Patchett, 1996; Vervoort et al., 1999; Amelin et al., 1999, 2000).

to 62 Ma with $\varepsilon Hf_{(t)}$ ranging from +6.7 to –27.0. These results are plotted against U-Pb age (Fig. 5A) for each sample, and in a composite density plot (Fig. 5B). For comparison purposes, the $\varepsilon Hf_{(t)}$ values are also summarized in Table 1 according to two age classifications: (1) Permian through Early Cretaceous ages (ca. 299 Ma through 100 Ma), and (2) Late Cretaceous through Paleogene ages (ca. 100 Ma through 55 Ma).

Figure 5B illustrates that most $\varepsilon Hf_{(t)}$ data from the San Juan Basin sample fall predominantly within two main groups, one in the Late Jurassic (ca. 165–160 Ma) with $\varepsilon Hf_{(t)}$ values ranging from +1 to –14, and the main cluster in the Late Cretaceous and Paleocene (ca. 79–62 Ma) with $\varepsilon Hf_{(t)}$ ranging from +7 to –15. A subordinate Triassic group is also present, with $\varepsilon Hf_{(t)}$ between +1 to –10.

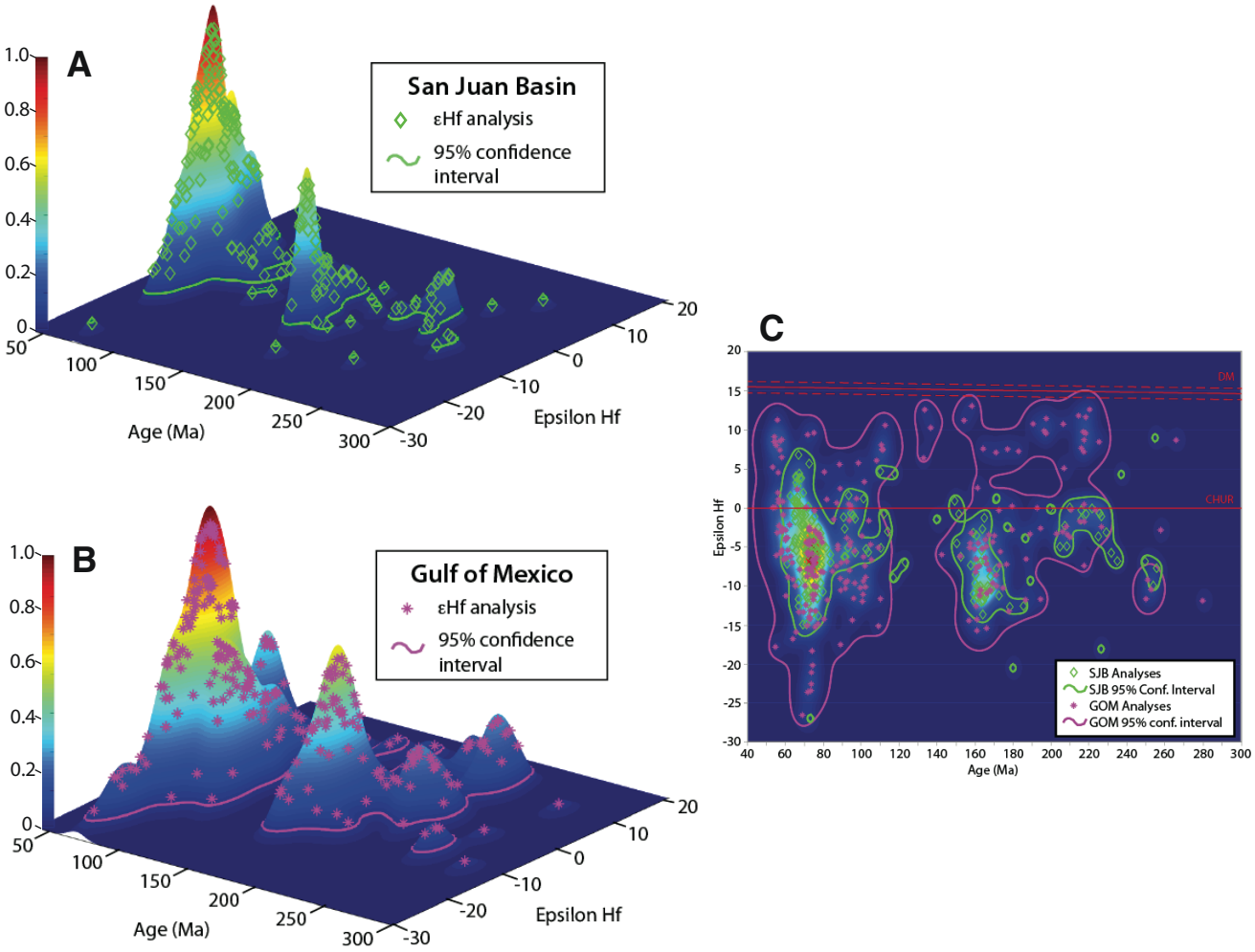

Figure 7. Epsilon hafnium vs. U-Pb age plots. (A) Three-dimensional scatter plot showing San Juan Basin detrital zircon samples. Green line is 95% confidence contour interval. (B) Three-dimensional scatter plot showing Wilcox Group, Gulf of Mexico Basin detrital zircon samples. Purple line is 95% confidence contour interval. (C) Two-dimensional scatter plot comparison of San Juan Basin (SJB) versus Gulf of Mexico Basin (GOM) samples. Green lines are 95% confidence contour intervals for San Juan Basin results. Purple lines are 95% confidence contour intervals for Gulf of Mexico results. Average crustal evolution arrow is based on $^{176}Lu/^{177}Hf$ ratio of 0.0115 (Vervoort and Patchett, 1996; Vervoort et al., 1999; Amelin et al., 1999, 2000). DM—depleted mantle reservoir reference from Vervoort and Blichert-Toft (1999); CHUR—chondritic uniform reservoir from Bouvier et al. (2008). All three plots were generated using HafniumPlotter (Matlab script) from Sundell et al. (2019). Values were plotted in three dimensions (parts A and B) and 95% density contour intervals were determined using HafniumPlotter (Sundell et al., 2019).

Gulf of Mexico Samples

We produced a total of 246 Lu-Hf laser analyses on the detrital zircon samples from the Wilcox Group. This included 110 zircons ranging in age from 280 Ma to 100 Ma with $\varepsilon Hf_{(t)}$ ranging from +13.0 to −15.8, and 136 zircons ranging in age from 99 Ma to 54 Ma with $\varepsilon Hf_{(t)}$ ranging from +11.2 to −26.6. These results are plotted against U-Pb age for each individual sample (Fig. 6A), and in a composite density plot (Fig. 6B). For ease of comparison, these $\varepsilon Hf_{(t)}$ values are also summarized in Table 1 according to the two age classifications as above.

The main cluster of Gulf of Mexico data exhibits a slight increase in $\varepsilon Hf_{(t)}$ values (less negative) from ca. 260 Ma (mean $\varepsilon Hf_{[t]} = -8$) to ca. 215 Ma (mean $\varepsilon Hf_{[t]} = -2$). The $\varepsilon Hf_{(t)}$ values hold steady ($\varepsilon Hf_{[t]} = -3$ to -4) from ca. 215 Ma to ca. 205 Ma, followed by a general decrease in $\varepsilon Hf_{(t)}$ (more negative) starting ca. 200 Ma and continuing until ca. 160 Ma ($\varepsilon Hf_{[t]}$ range from ~0 to −16, mean = −8).

DISCUSSION

Cretaceous and Paleogene detrital zircon provenance of both the San Juan and Gulf of Mexico Basins has been the focus of many recent studies (Mackey et al., 2012; Blum and Pecha, 2014; Wahl et al., 2016; Blum et al., 2017; Pecha et al., 2018; Smith et al., 2020). The addition of Hf isotope geochemistry on zircons from both regions allows further examination of their respective provenance, including evaluation of their genetic relationship,

Table 1. SUMMARY OF DETRITAL ZIRCON EPSILON Hf RESULTS

Sample no.	Unit name	Permian through Early Cretaceous zircons			Late Cretaceous through Paleocene zircons		
		U-Pb age range (Ma)	No. of zircons	Epsilon Hf isotopic composition	U-Pb age range (Ma)	No. of zircons	Epsilon Hf isotopic composition
San Juan Basin samples							
WP-34	Nacimiento Fm.	230–124	14	–0.2 to –12.7	92–62	11	–4.0 to –27.0
WP-45	Animas Fm.	225–162	5	–3.7 to –13.7	94–63	20	+1.5 to –15.0
WP-56	McDermott Fm. (upper)	N/A*	0	+6.7 to –4.9	70–66	15	+6.7 to –4.9
WP-53	McDermott Fm. (basal)	250–164	4	–6.9 to –12.1	80–66	13	+0.2 to –13.9
WP-54	Kirtland Fm.	256–112	7	–0.1 to –13.7	97–72	5	–5.8 to –15.0
WP-31	Fruitland Fm.	227–161	8	–1.5 to –20.6	95–66	23	+0.1 to –10.0
WP-24	Cliff House Sandstone	254–103	22	+1.2 to –12.0	96–77	6	+1.6 to –11.6
WP-39	Pictured Cliffs Sandstone	255–102	14	+8.9 to –12.8	97–73	26	+5.6 to –10.7
San Juan Basin composite		256–102	74	+8.9 to –20.6	97–62	119	+6.7 to –27.0
Gulf of Mexico samples							
GOM-76	Wilcox Group	219–103	18	+13.0 to –15.8	94–54	18	+8.7 to –17.9
GOM-46	Wilcox Group	226–109	14	+12.6 to –6.6	81–55	11	+9.1 to –8.3
GOM-71	Wilcox Group	253–101	29	+12.5 to –14.5	97–56	45	+11.2 to –23.5
GOM-70	Wilcox Group	266–102	25	+10.5 to –15.2	99–57	32	+9.6 to –23.7
GOM-67	Wilcox Group	280–100	24	+7.5 to –15.5	98–61	30	+1.1 to –26.6
Gulf of Mexico composite		280–100	110	+13.0 to –15.8	99–54	136	+11.2 to –26.6

*N/A—not applicable.

TABLE 2. DETRITAL ZIRCON Hf SIGNATURES OF THE NORTH AMERICAN CORDILLERAN MAGMATIC ARC

Region	Permian through Early Cretaceous zircons		Late Cretaceous through Paleocene zircons		References
	U-Pb age range (Ma)	Epsilon Hf isotopic composition	U-Pb age range (Ma)	Epsilon Hf isotopic composition	
Coast Mountains batholith/Coast plutonic complex (CPC)	153–101	+12.3 to +2.6	97–5	+11.6 to +1.5	Cecil et al. (2011)
North Cascades Range (NC)	268–101	+14.0 to –0.9	99–69	+5.9 to –22.5	Sauer et al. (2017)
Idaho batholith (IB)	N/A*	N/A*	99–55	–8.7 to –26.5	Gaschnig et al. (2011)
Sierra Nevada batholith (SN)	121–102	+11.8 to –4.7	99–70	+11.8 to –4.7	Lackey et al. (2012)
Porphyry copper province (PCP)	234–100	+5.5 to –35.7	97–54	–2.3 to –24.9	Fisher et al. (2017); Chapman et al. (2018)
Sierra Madre Occidental (SMO)	288–239	–2.0 to –34.9	89–53	+8.9 to –12.8	Arvizu and Iriondo (2011); Mahar et al. (2016)
Peninsular Ranges (PR)	273–100	+12.1 to –2.6	98–87	+11.5 to –21.3	Shaw et al. (2014)
Transverse Ranges (TR)	242–117	–5.0 to –23.0	89–67	–2.2 to –25.7	Barth et al. (2016); Fisher et al. (2017)

*N/A—not applicable.

and it allows for testing/refinement of previous paleogeographic models. Below, we establish the Hf isotopic signatures of both basins and then compare the results to each other and the eight principal elements of the North American Cordilleran magmatic arc. Finally, we use these comparisons to refine previous Gulf of Mexico drainage models (Galloway et al., 2011; Blum et al., 2017) during late Paleocene time.

Limiting the Lu-Hf portion of the study to zircons with a $^{206}Pb/^{238}U$ age younger than 300 Ma and to drainage embayments that are known to have received sediment from western North American sources (e.g., Cordilleran orogenic belt) bolstered our chances of robust provenance assessment. Eight samples from the San Juan Basin were chosen for Lu-Hf isotopic analysis; of these, three (WP 39 Pictured Cliffs Sandstone, WP24 Cliff House Sandstone, and WP 31 Fruitland Formation) are known to have provenance ties to the Laramide porphyry copper province in southern Arizona and southwestern New Mexico, two (WP 54 Kirtland Formation and WP 34 Nacimiento Formation) are thought to be mainly reworked from older Mesozoic units, and three have known provenance ties to the nearby Colorado Mineral Belt (Donahue, 2016; Pecha et al., 2018). Samples chosen for Lu-Hf analysis from the Wilcox Group strata exposed in the coastal regions of the Gulf of Mexico Basin included five with known provenance ties to the Cordilleran orogenic belt (Blum and Pecha, 2014; Blum et al., 2017). Samples GOM-76 and GOM-46 came from central Arkansas and are thought to have a more northerly sourced provenance that would have originated in the midcontinent region, including parts of the Appalachian highlands (based on reconstructions of Sharman et al., 2017) or the northern Rocky Mountains region via the paleo–Platte River, including the Idaho batholith and elevated Nevadaplano regions (based on reconstructions of Blum et al., 2017). Samples GOM-71, GOM-70, and GOM-67 came from the Simsboro Formation in east Texas and are thought to be derived from the southwestern reaches of the Cordillera, specifically, New Mexico, Arizona, and the greater Four Corners region (Blum and Pecha, 2014; Blum et al., 2017).

Hf Signature of San Juan Basin Sediments

The Hf isotopic signature of Late Cretaceous through Paleocene detrital zircons of the San Juan Basin is distinctive, with three increases and two decreases in $\varepsilon Hf_{(t)}$ (Fig. 5). Tracking deviations in $\varepsilon Hf_{(t)}$ from average crustal evolution over time (Fig. 5A) from 300 to 40 Ma was done by calculating a running average (bin width of five analyses). An increase from −10 to 0 in $\varepsilon Hf_{(t)}$ space occurred from ca. 260 to 220 Ma, followed by a decrease to ~−13 by ca. 180 Ma. A dramatic increase from −14 to +1 in $\varepsilon Hf_{(t)}$ occurred at ca. 160 Ma, followed by average crustal $^{176}Lu/^{177}Hf$ evolution until ca. 80 Ma, when another decrease occurred to $\varepsilon Hf_{(t)}$ of ~−15 (with an outlier at −27). The final increase occurred ca. 75–64 Ma, when $\varepsilon Hf_{(t)}$ ranged from ~−15 to +7.

These new Hf data support earlier U-Pb detrital zircon provenance assignments from Donahue (2016) and Pecha et al. (2018). Late Cretaceous samples from the Pictured Cliffs Sandstone, Cliff House Sandstone, and Fruitland Formation (WP39, WP24, WP31, respectively) are indistinguishable in terms of their $\varepsilon Hf_{(t)}$ values (Fig. 5A). This supports the suggestion proposed by Pecha et al. (2018) that these units were derived from similar sources southwest of the San Juan Basin. Based on U-Pb ages of detrital zircons and paleocurrent indicators, these units have been interpreted to have provenance ties to the Mogollon Highlands and the porphyry copper province of southern Arizona and southwestern New Mexico (Pecha et al., 2018).

Within the San Juan Basin sequence, the Maastrichtian McDermott Formation (WP53, WP56) and Lower–Middle Paleocene Animas Formation (WP45) were identified as the best candidates for characterizing Colorado Mineral Belt input into the basin. It was necessary to use these detrital samples as a proxy for igneous rocks of the Colorado Mineral Belt due to the complete lack of zircon Hf analyses from igneous rocks of the Colorado Mineral Belt. The fluvial volcaniclastic McDermott Formation (Reeside, 1924; McCormick, 1950; Barnes et al., 1954; Kottlowski, 1957; Sikkink, 1987; O'Shea, 2009; Gonzales, 2010) was deposited on the southern periphery of the Colorado Mineral Belt, along the northern margin of the San Juan Basin. Gonzales (2010) recognized that the McDermott Formation likely represents a roof-flank detachment deposit, which incorporated debris flows and fluvial sedimentation. The Animas Formation is a volcanic-rich fluvial sandstone, with paleocurrent indicators toward the southeast, directly from southern Colorado Mineral Belt sources, including the LaPlata Mountains laccolithic complex (Fassett, 1985; Gonzales, 2010; Pecha et al., 2018; Cather et al., 2019). The areal extent of both units is restricted to the northwestern portion of the San Juan Basin near Durango, Colorado, which lies immediately adjacent to the Needle Mountains uplift and the southern segment of the Colorado Mineral Belt, and likely only sampled the southern portion of the Colorado Mineral Belt (Fig. 2). The central and northern parts of the Colorado Mineral Belt remain uncharacterized for zircon Hf isotopes but still likely contributed sediment to the Gulf of Mexico Basin.

San Juan Basin Epsilon Hf Proxy

Insofar as most of the Cretaceous strata that once blanketed the uplifted Colorado Plateau region have been removed by erosion, we developed a proxy for these sediments, in terms of zircon $\varepsilon Hf_{(t)}$ values, based on preserved San Juan Basin sediments (Fig. 5). This proxy, including the running average of $\varepsilon Hf_{(t)}$, can now be used as a reference for this and future detrital zircon provenance comparisons and assignments.

Hf Signature of Gulf of Mexico (Paleocene Wilcox Formation) Sediments

Two distinct trends in $\varepsilon Hf_{(t)}$ are noted in the Gulf of Mexico samples (Fig. 6A) during Permian through Early Cretaceous time: (1) a main cluster (ca. 280–145 Ma) ranging from 0 to −16 $\varepsilon Hf_{(t)}$, and (2) a subordinate group (ca. 225–130 Ma) ranging from

+13 to +5 $\varepsilon Hf_{(t)}$. Running mean averages (dashed and solid black lines in Fig. 6A) clearly display these two trends in $\varepsilon Hf_{(t)}$ space. These two trends suggest the Wilcox Group sediments were likely derived from two regions with distinct crustal evolution characteristics. The main cluster of data is consistent with magmatic recycling of primarily Proterozoic, and, to a lesser extent, Archean crust, whether via first-cycle erosion or sedimentary recycling. The subordinate and more juvenile $\varepsilon Hf_{(t)}$ cluster is consistent with derivation from juvenile crust. This idea is explored later in this discussion, where we compare our results with the varying tectonic elements of the North American Cordillera.

Samples GOM-46 and GOM-76 are late Paleocene to earliest Eocene and were deposited in fluvial deltaic plains that have previously been interpreted to represent part of the paleo-Mississippi drainage and paleo-Arkansas drainage, respectively, and that entered the Gulf of Mexico Basin through the Mississippi embayment (Galloway et al., 2000, 2011; Jackson et al., 2021; Blum and Pecha, 2014; Blum et al., 2017; Sharman et al., 2017). Samples GOM-67, GOM-70, and GOM-71 are from late Paleocene to earliest Eocene sandstones deposited in analogous depositional systems, but they represent paleo–Brazos River/paleo–Colorado River deposition (Loucks et al., 1986; Hamlin, 1988; Galloway et al., 2000, 2011; Jackson et al., 2021; Blum and Pecha, 2014; Blum et al., 2017; Sharman et al., 2017). Sediment routing to the Gulf of Mexico Basin for these three samples was through the Houston embayment (Blum and Pecha, 2014; Blum et al., 2017; Sharman et al., 2017). Paleocene depositional environments were analogous to the Pleistocene–modern Gulf of Mexico coastal plain depositional environments (Blum and Price, 1988; Blum and Aslan, 2006; Galloway, 2008; Galloway et al., 2011).

To establish an $\varepsilon Hf_{(t)}$ signature of the Wilcox Group sediments during the late Paleocene to early Eocene, we grouped all five Gulf of Mexico samples together and plotted the data using density contour intervals (Fig. 6B). From these data, it is clear that there are two main groupings: (1) from ca. 230 to ca. 140 Ma with $\varepsilon Hf_{(t)}$ ranging from +1 to −16, and (2) from ca. 110 to ca. 55 Ma with $\varepsilon Hf_{(t)}$ ranging from +3 to −27. We also observe a juvenile trend in the data that spans the entire age range from ca. 230 Ma to ca. 55 Ma with $\varepsilon Hf_{(t)}$ ranging from +15 to +5. The differentiation of these isotopic signatures holds important implications for provenance assessments of Gulf of Mexico sediments.

Comparison of San Juan Basin and Gulf of Mexico Hf Signatures

The effects of Laramide tectonism on sedimentation in the Gulf of Mexico have been noted by several previous researchers (Dickinson et al., 1988; Lawton, 2008; Galloway et al., 2011; Mackey et al., 2012; Blum and Pecha, 2014). Laramide basement-cored uplifts and their overlying sedimentary blanket in the Rocky Mountains have been interpreted as the primary sediment sources of the Wilcox Group in the Gulf of Mexico Basin (Galloway et al., 2011; Mackey et al., 2012). The Lower Wilcox Group in south Texas contains Cordilleran magmatic arc–derived detritus, whereas the Upper Wilcox Group is enriched in basement and recycled sedimentary cover detritus (Mackey et al., 2012). Drainage reorganization (Blum and Pecha, 2014) or drainage area capture (Sharman et al., 2017) likely contributed to the marked increase in sedimentation rate that is observed in the Lower Wilcox Group during late Paleocene time. Another explanation for the increased rate of sediment accumulation in the Lower Wilcox Group is rapid erosion of relatively soft sedimentary rocks, particularly the Mesozoic section that once covered the Laramide basement-cored uplifts (Galloway et al., 2011).

The relationship between the San Juan Basin proxy for the eroded sedimentary cover that was shed from uplifting Laramide blocks and the Gulf of Mexico sediments is clearly illustrated by directly comparing their $\varepsilon Hf_{(t)}$ results (Fig. 7). By draping the scatter plot on the three-dimensional density plot, it becomes evident that the ratios among Triassic, Jurassic, and Cretaceous analyses are consistent between the two regions. Similar isotopic decreases in both Jurassic and Late Cretaceous zircons point to a shared provenance between the two regions. There is also a marked similarity in $\varepsilon Hf_{(t)}$ between the San Juan Basin and Gulf of Mexico data sets when plotted in two dimensions (Fig. 7C), where the overlap between the regions at the 95% confidence interval is evident. However, this similarity is restricted to the more evolved "main" portion of the Gulf of Mexico signature ($\varepsilon Hf_{[t]}$ = 0 to −16) and is clearly distinct from the juvenile portion ($\varepsilon Hf_{[t]}$ = +13 to +5). From these data, we interpret a possible (perhaps even likely) connection between San Juan Basin and Gulf of Mexico sediment pathways, supporting the notion of Galloway et al. (2011), who suggested that increased depositional rates in the Lower Wilcox Group likely represent a combination of drainage area capture (Sharman et al., 2017) and the erosion of the easily weathered sedimentary cover that once blanketed the basement-cored Laramide-aged uplifts.

With documented exit points to the San Juan Basin in the east and southeast (Cather, 2004; Cather et al., 2019) portions of the basin, expectations are that Wilcox Group sediments deposited through the Houston embayment should record sediments derived from Colorado Mineral Belt sources. The abundance of volcanic detritus in parts of the Wilcox Group also points to the Colorado Mineral Belt as a potential source (Galloway et al., 2011). However, the Colorado Mineral Belt $\varepsilon Hf_{(t)}$ signature is nearly nonexistent within the Wilcox Group samples analyzed. Two plausible explanations exist for this apparent absence. (1) Specific units in the San Juan Basin known to include Colorado Mineral Belt detritus, the McDermott and Animas Formations, sequestered all the detritus from the Colorado Mineral Belt, and very little, if any, of this material exited the San Juan Basin. This is possible because both units are restricted spatially to the northern perimeter of the basin, and neither exists in the axial portions of the basin or near the exit points on the east and southeast. (2) The various plutons and laccoliths in the southern half of the Colorado Mineral Belt contain large amounts of xenocrystic zircons and very few zircons exhibiting crystallization ages (Gonzales, 2015). U-Pb age spectra from Late Cretaceous

to Paleogene strata of the Denver Basin only show minimal input from the nearby Colorado Mineral Belt sources, as represented with a small age peak at ca. 65 Ma (Sharman et al., this volume).

Although potential source regions in the eastern United States were also considered during this evaluation, they were ruled out for two main reasons: (1) the absence of Paleocene clastic sedimentation along the Atlantic perimeter (Poag and Sevon, 1989; Galloway et al., 2011), and (2) the lack of volcanic source regions east of the Mississippi River that could account for the zircons younger than 300 Ma and the abundant volcanogenic components found within in the Wilcox Group (Galloway et al., 2011).

COMPARISONS TO THE CORDILLERAN MAGMATIC ARC

Cordilleran Magmatic Arc Hf Signal

Detrital zircon studies have revolutionized provenance studies (Gehrels, 2012), mainly because samples restricted to a specific region often contain information that pertains to a much larger region and/or tectonic process. A similar narrative pertains to this study, where zircons sequestered within the San Juan and Gulf of Mexico Basins provide information about the crustal evolution of the distant Cordilleran magmatic arc during the 285–51 Ma time frame. Whereas Cordilleran magmatism continued until Miocene time, we only considered magmatism that occurred until 51.1 Ma, the minimum age of the Wilcox Group (Zarra et al., 2019).

To evaluate sediment provenance, comparisons of our new San Juan Basin and Gulf of Mexico $\varepsilon Hf_{(t)}$ data were made with reference hafnium data sets from the eight principal tectonic elements that comprise the North American Cordilleran magmatic arc (Figs. 8 and 9).

Comparisons with the Southern Segment of the North American Cordilleran Arc

Figure 8 compares our new $\varepsilon Hf_{(t)}$ data to the four major magmatic provinces of the Cordilleran arc, including the southwestern Laramide porphyry copper province (Fig. 8A), Sierra Madre Occidental (Fig. 8B), Peninsular Ranges (Fig. 8C), and Transverse Ranges (Fig. 8D).

Significant proportions of both the San Juan Basin and Gulf of Mexico Basin zircons likely have provenance ties to the Laramide porphyry copper province. This includes matches in $\varepsilon Hf_{(t)}$ space for Jurassic grains (ca. 180–145 Ma), Cretaceous grains (ca. 110–65 Ma), and Paleocene grains (ca. 65–58 Ma). This is not surprising, because Pecha et al. (2018) indicated that the Upper Cretaceous units (Pictured Cliffs Sandstone through the Fruitland Formation) in the San Juan Basin were predominantly derived from southwest North America, as northeast-flowing rivers exited the Mogollon Highlands region. As the Laramide basement block uplifts in the Four Corners region began to rise during latest Cretaceous and Paleocene time, the overlying Mesozoic strata would have been easily stripped off and deposited in available accommodation space in one of the intervening Laramide-aged intraforeland basins (e.g., Denver Basin) or in lacustrine environments (e.g., Green River Basin), or this sediment made its way to the Gulf of Mexico Basin, ultimately to be deposited as Wilcox Group strata.

The Transverse Ranges of California are an unlikely sediment source to the Gulf of Mexico because they are thought to be sediment sources to the forearc to their west (i.e., Jacobson et al., 2011; Sharman et al., 2015). However, for a complete evaluation of potential sources in the North American Cordillera, they were compared with our new data from the San Juan and Gulf of Mexico Basins (Fig. 8D). The potential contribution from this region would be the evolved Late Cretaceous (ca. 80 Ma to 65 Ma) zircons with $\varepsilon Hf_{(t)}$ values ranging from approximately −5 to −20. The Peninsular Ranges are also known to have west-flowing drainages during late Paleocene and Eocene time (Jacobson et al., 2011; Sharman et al., 2015), but they were also included in the comparisons in the event that east-flowing drainages also existed. However, both the Peninsular Ranges and the Sierra Madre Occidental components of the magmatic arc are poor matches for the zircons found in the San Juan Basin and Gulf of Mexico samples. Other than the partial overlap in Late Cretaceous juvenile to intermediate zircons (ranging from +12 to +2), these regions do not appear to have been major contributors to the overall sediment supply entering either the San Juan Basin or the central Gulf of Mexico Basin through the Houston embayment or the Mississippi embayment. Both regions lie to the southwest of previously defined drainage areas flowing to the central Gulf Coast region (Fig. 4), and if tapped, they would have likely entered the Gulf of Mexico through the paleo–Rio Grande/Rio Grande embayment (Figs. 3 and 4), which is not included in this study.

Based on previously published data, the juvenile $\varepsilon Hf_{(t)}$ signature (older than ca. 125 Ma) in zircons from the Gulf of Mexico could not have been generated from any of the four magmatic provinces in the southern section of the Cordilleran magmatic arc.

Comparisons with the Northern Segment of the North American Cordilleran Arc

Figure 9 compares our $\varepsilon Hf_{(t)}$ data with the four principal magmatic arc segments in the northern portion of the Cordillera, which include the Coast Mountains batholith (Fig. 9A), North Cascades Range (Fig. 9B), Idaho batholith (Fig. 9C), and Sierra Nevada batholith (Fig. 9D).

Comparisons to both the Coast Mountains batholith and the North Cascades Range provide a compelling argument that these regions have provenance ties to the Gulf of Mexico. The Coast Mountains batholith is the only region that provides a potential source for the Late Triassic and Early Jurassic juvenile zircons in the Wilcox Group. A combination of the Coast Mountains batholith and North Cascades Range can account for most of the juvenile input to the Wilcox Group samples that entered the Gulf Coast region through the Mississippi embayment.

The Late Cretaceous decrease in $\varepsilon Hf_{(t)}$ values observed in the Gulf of Mexico samples (Fig. 9C) provides compelling evidence of a connection to the Idaho batholith. The $\varepsilon Hf_{(t)}$ increase from –10 to 0 observed in these same samples during the Paleocene also suggests a connection to the Idaho batholith. However, only input from the Coast Mountains batholith or the Sierra Madre Occidental can explain the juvenile part of the Paleogene $\varepsilon Hf_{(t)}$ increase.

Comparisons to the Sierra Nevada batholith provide poor provenance ties with both the San Juan Basin and Gulf of Mexico samples (Fig. 9D). However, the Sierra Nevada batholith is likely undercharacterized with respect to Hf isotopes in zircon, as the only published data are from a limited number of samples reported by Lackey et al. (2012). There are juvenile $\varepsilon Hf_{(t)}$ values ranging from +12 to +5 within the current Sierra Nevada batholith data set, but they are sparse and limited in age range from ca. 120 Ma to ca. 100 Ma. Even if there were additional juvenile components within the batholith, numerous lines of evidence indicate they likely would not be included in the Gulf of Mexico drainage headwaters. The presence of a well-established paleodrainage divide during Late Cretaceous and early Paleogene times (Henry, 2008; Lechler and Niemi, 2011; Cassel et al., 2012; Sharman et al., 2015) precludes the tapping of Sierra Nevada batholith sources by Gulf of Mexico drainage headwaters. An

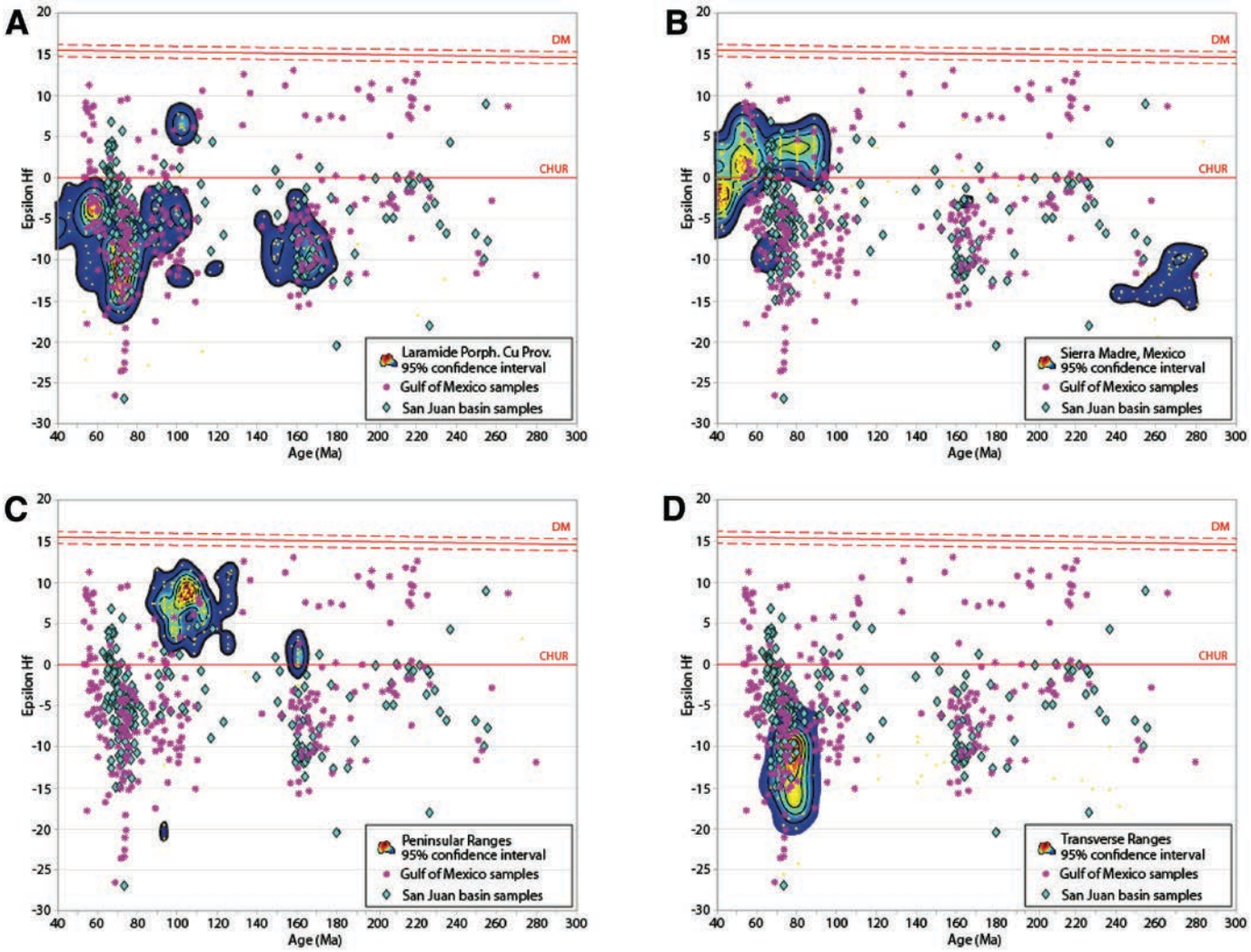

Figure 8. Epsilon Hf comparison plots with four of the principal tectonic elements of the southern North American Cordilleran magmatic arc. San Juan Basin and Gulf of Mexico $\varepsilon Hf_{(t)}$ results were plotted over bivariate kernel density estimates from previously published epsilon Hf results as follows: (A) Laramide porphyry copper province of southern Arizona, southwestern New Mexico, and southeastern (Mojave region) California from Fisher et al. (2017) and Chapman et al. (2018); (B) Sierra Madre, Mexico, from Arvizu and Iriondo (2011), Mahar et al. (2016), and Garcia et al. (2021); (C) Peninsular Ranges batholith from Shaw et al. (2014); and (D) Transverse Ranges from Barth et al. (2016) and Fisher et al. (2017). Density plot was generated using HafniumPlotter (Matlab script) from Sundell et al. (2019), with black contour representing 95% density contour. DM—depleted mantle reservoir reference from Vervoort and Blichert-Toft (1999); CHUR—chondritic uniform reservoir from Bouvier et al. (2008).

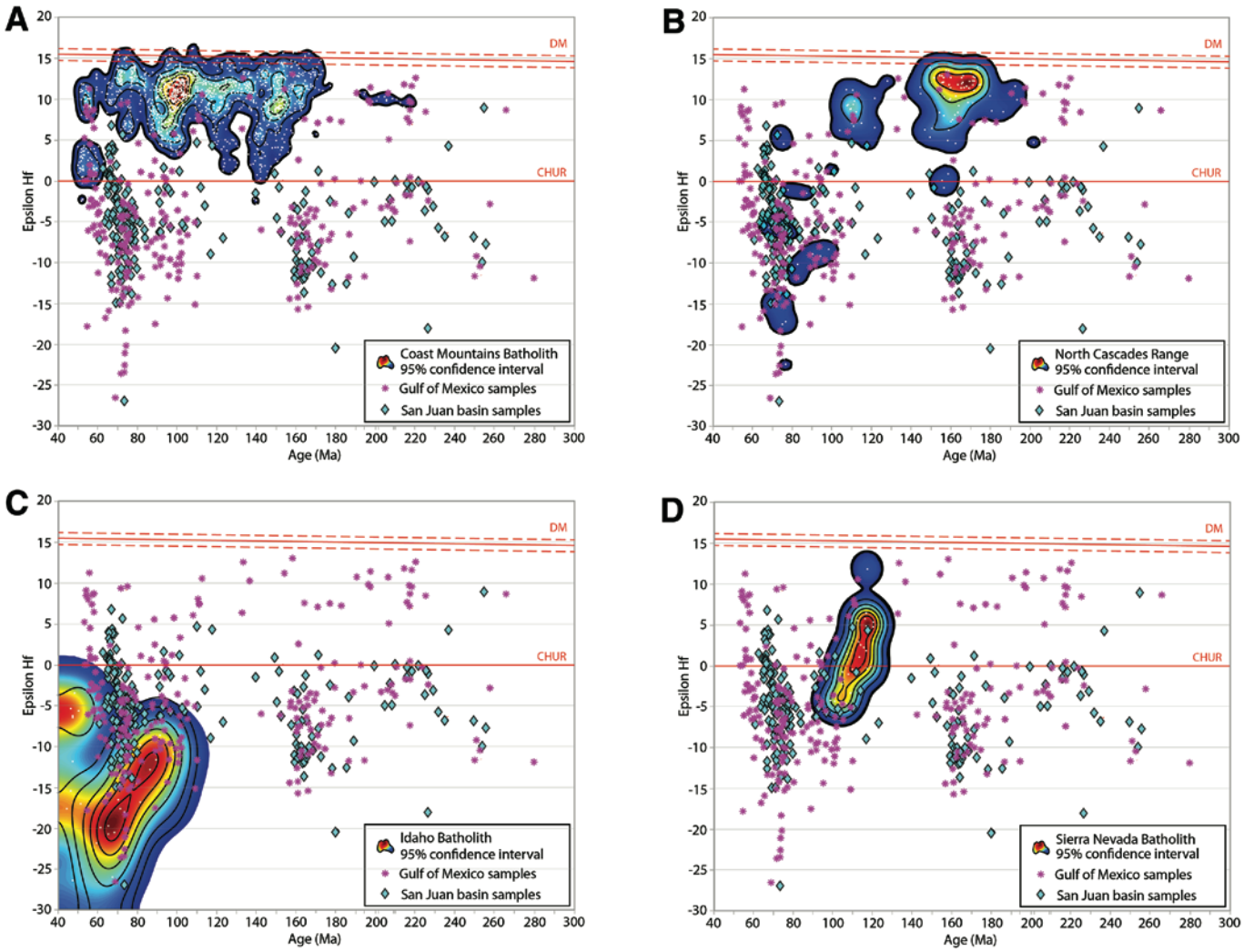

Figure 9. Epsilon Hf comparison plot with four of the principal tectonic elements of the northern North American Cordilleran magmatic arc. San Juan Basin and Gulf of Mexico $\varepsilon Hf_{(t)}$ results were plotted over bivariate kernel density estimates from previously published epsilon Hf results as follows: (A) Coast Mountains batholith, southeastern Alaska and coastal British Columbia, Canada, from Cecil et al. (2011), Homan (2017), and Dafov et al. (2020); (B) North Cascades Range from Sauer et al. (2017); (C) Idaho batholith from Gaschnig et al. (2011); and (D) Sierra Nevada batholith from Lackey et al. (2012). Density plot was generated using HafniumPlotter (Matlab script) from Sundell et al. (2019), with black contour representing 95% density contour. DM—depleted mantle reservoir reference from Vervoort and Blichert-Toft (1999); CHUR—chondritic uniform reservoir from Bouvier et al. (2008).

eastward migration of Sierra Nevada forearc drainages during Maastrichtian through Paleocene time also precludes detritus from the batholith being able to enter the Gulf of Mexico drainage network (Sharman et al., 2015).

After evaluating the potential provenance ties from all eight regions, it is evident the Wilcox Group has provenance ties to multiple elements of the Cordilleran arc. The most likely sources of the more evolved zircons ($\varepsilon Hf_{[t]}$ ranging from 0 to −27) are the Laramide porphyry copper province and the Idaho batholith. The more juvenile zircons ($\varepsilon Hf_{[t]}$ ranging from +11.2 to 0) were probably derived from the Coast Mountains batholith and, to a lesser extent, the North Cascades Range.

Insights into the Triassic through Early Cretaceous Magmatic Arc

As described earlier, similar $\varepsilon Hf_{(t)}$ results for the Gulf of Mexico and San Juan Basins indicate they likely shared some of the same source regions (e.g., Laramide porphyry copper province). However, an important distinction between the two distributions occurs in the San Juan basin samples, which do not contain the juvenile trend ($\varepsilon Hf_{[t]}$ = +5 to +13 from ca. 270 to ca. 100 Ma) that is prominently displayed by a subset of the Gulf of Mexico samples (GOM-76 and GOM-46). This indicates that the more juvenile zircons were not routed to the Gulf of Mexico

through the San Juan Basin and must have entered the Gulf of Mexico drainage network through a different pathway. The Coast Mountains batholith and the North Cascades Range (Figs. 7A and 7B, respectively) provide the only two known source regions within the North American Cordillera that contain zircons with juvenile $\varepsilon Hf_{(t)}$ ranging from +5 to +13 encompassing the entire age range of ca. 200 to ca. 100 Ma. The Coast Mountains batholith is the only known source for the distinctive juvenile zircons ($\varepsilon Hf_{[t]}$ = +5 to +13) from both ca. 230 to ca. 190 Ma, and also from ca. 100 to ca. 51 Ma.

The Jurassic (ca. 200 to ca. 160 Ma) decrease in $\varepsilon Hf_{(t)}$ values observed in San Juan Basin, Gulf of Mexico Basin, and Laramide porphyry copper province samples (Fig. 8A) indicates magmatic recycling of Proterozoic or older crust. This deviation toward more negative $\varepsilon Hf_{(t)}$ values indicates either a migration of the Jurassic magmatic arc into older continental crust with time or crustal thickening events that increased the proportion of crustal material in the melts. Late Triassic to early Middle Jurassic magmatism in both the Klamath-Sierran and Mojave-Sonoran segments could have been the source of these zircons with evolved Hf signatures ($\varepsilon Hf_{[t]}$ = 0 to −15). However, during Middle to Late Jurassic time, these two segments of the arc began to differ in character, when shortening in the Klamath-Sierran segment began to thicken the crust (Busby-Spera et al., 1990). A possible scenario is that the Late Jurassic decrease in $\varepsilon Hf_{(t)}$ in both San Juan Basin and Gulf of Mexico samples was related to thickening of the crust in the Klamath-Sierran segment of the arc, but this pattern is not evident in the comparison plot (Fig. 7D) because of limited Hf isotopic data from the Sierra Nevada. Alternatively, crustal thickening events in the Jurassic arc may have extended southward into the Mojave-Sonora region. This latter interpretation fits best with detrital zircon provenance interpretations for Cretaceous strata of the San Juan Basin (Pecha et al., 2018), and it is supported by our new $\varepsilon Hf_{(t)}$ data, which indicate provenance ties to the Laramide porphyry copper province of southern Arizona and southwestern New Mexico (Fig. 8A). However, it is difficult to reconstruct crustal thickening events in this segment of the arc due to dissection of the region by Cenozoic Laramide and extensional tectonic events. This is supported by the fact that San Juan Basin sediments (Figs. 5 and 7) display $\varepsilon Hf_{(t)}$ decreases similar in scale and duration during the same time interval.

The subordinate more juvenile grouping (εHf = +13 to +5) in the Wilcox Group does not display εHf increases or decreases; instead, εHf follows the trend of average $^{176}Lu/^{177}Hf$ crustal evolution from ca. 260 Ma to ca. 100 Ma. These juvenile zircons are not found in any San Juan Basin samples, which means they were not being routed to the Gulf of Mexico through the Four Corners region.

Insights into the Late Cretaceous and Paleocene Magmatic Arc

Coeval $\varepsilon Hf_{(t)}$ decreases (minimum $\varepsilon Hf_{[t]}$ of –27 from ca. 74 to 69 Ma) are present in both the San Juan Basin and Gulf of Mexico Basin samples and represent magmatic recycling of Proterozoic and/or Archean crust into the melt that crystallized these zircons. These decreases likely represent migration of the Sevier-Laramide magmatic arc inland toward the interior of the North American craton into older basement crust. Immediately following this decrease, both data sets reveal progressive increases in $\varepsilon Hf_{(t)}$. Within the San Juan Basin samples, a distinct increase from −8 to +6.7 in $\varepsilon Hf_{(t)}$ begins at ca. 68 Ma and continues to ca. 62 Ma. Based on provenance interpretations of Donahue (2016) and Pecha et al. (2018), the zircons that form this increase were derived from the Colorado Mineral Belt, which is located just north of the San Juan Basin. The basement within this region is principally composed of Paleoproterozoic Yavapai-Mazatzal crust (Whitmeyer and Karlstom, 2007), so this indicates there was a substantial input of juvenile material incorporated into the melts that generated these zircons. Within the Gulf of Mexico samples, the $\varepsilon Hf_{(t)}$ increase also begins around 68 Ma, but it is offset in age from the San Juan Basin data by ~6 m.y., reaching its maximum of +11 by 56 Ma.

Defining the Epsilon Hf Signature for Laramide-Age (ca. 85–50 Ma) Zircons

One of the results from the new data set, and the accompanying compilation of previously published Hf isotopic data, is a Laramide-age detrital zircon $\varepsilon Hf_{(t)}$ versus U-Pb age source plot (Fig. 10). The varying isotopic character of Laramide magmatism, based on location within the arc, allows for differentiation of sediment source(s) of zircons ranging in age from ca. 85 to ca. 50 Ma. While there is some overlap among certain source fields, potential provenance ties can typically be narrowed down to one or two source regions for most of the detrital zircons generated during this specific time span. Zircons from the Sierra Nevada batholith are notably absent on this diagram because this segment of the magmatic arc was extinguished by flat-slab subduction during the Laramide orogeny (e.g., Coney and Reynolds, 1977; Constenius et al., 2003).

The variability in Hf isotopic character of Laramide-age zircons appears to be primarily a function of basement geology and variable tectonic partitioning along the length of the North American Cordillera. For instance, inboard migration of magmatism into Precambrian basement within the central part of the orogen, classic retro-arc thin-skinned thrusting in the Central Mexico fold-and-thrust belt, and emplacement of juvenile magmas in isotopically juvenile crust in the Coast Mountains batholith are some of the perturbations in tectonic style that contributed to the Hf isotopic character. Based on the average crustal evolution $^{176}Lu/^{177}Hf$ ratio of 0.0115 (Vervoort and Patchett, 1996; Vervoort et al., 1999; Amelin et al., 1999, 2000), the resulting $\varepsilon Hf_{(t)}$ signatures during this time frame fall into three distinct groups: (1) values from +15 to +5 represent the influx of mantle-derived material and generation of juvenile crust, (2) values from +5 to −20 represent recycling of Proterozoic crust, and (3) values from −20 to −40 represent recycling of Archean crust.

Source regions that predominantly contain zircon with more juvenile to intermediate $\varepsilon Hf_{(t)}$ values are the Coast Mountains

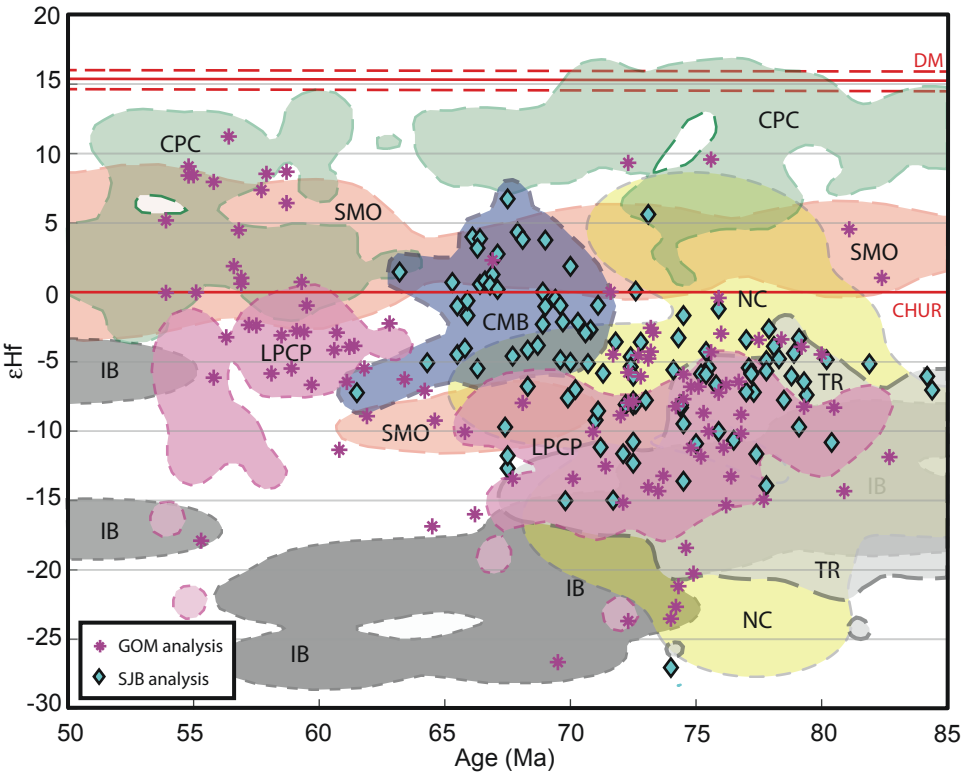

Figure 10. Epsilon Hf signatures of potential Laramide (ca. 85–50 Ma) source regions within the North American Cordillera. Reference comparisons: IB—Idaho batholith (Gaschnig et al., 2011); LPCP—Laramide porphyry copper province of southern Arizona, southwestern New Mexico, and southeastern California (Mohave region) (Fisher et al., 2017; Chapman et al., 2018); SMO—Sierra Madre Occidental (Arvizu and Iriondo, 2011; Mahar et al., 2016; Garcia et al., 2021); TR—Transverse Ranges (Barth et al., 2016); CMB—Colorado Mineral Belt (this study); CPC—Coast plutonic complex/Coast Mountains batholith (Cecil et al., 2011; Homan, 2017; Dafov et al., 2020); and NC—North Cascades Range (Sauer et al., 2017). Colored fields represent bivariate kernel density estimates based on 95% density contours generated by HafniumPlotter (Sundell et al., 2019). Scatter plot overlays epsilon Hf analyses from this study as follows: purple asterisk signs are from the Wilcox Group, Gulf of Mexico analyses (GOM), and blue diamonds are from San Juan Basin analyses (SJB). Colored Mineral Belt field is defined from detrital zircon $\varepsilon Hf_{(t)}$ values from the Animas Formation/McDermott Member in the San Juan Basin only, due to the lack of zircon Hf analyses on igneous zircon samples from other areas of the Colorado Mineral Belt. North Cascades Range field is defined from detrital zircon $\varepsilon Hf_{(t)}$ values from Mesozoic sedimentary rocks located adjacent to the southern North Cascades only, due to the lack of zircon Hf analyses on igneous zircon samples from other North Cascades Range igneous units. DM—depleted mantle reservoir reference from Vervoort and Blichert-Toft (1999); CHUR—chondritic uniform reservoir from Bouvier et al. (2008).

batholith (range +16 to −3), North Cascades Range, Sierra Madre Occidental (range +9 to −3, and −7 to −12 from 70 to 60 Ma), and the Colorado Mineral Belt (range +7 to −7). Zircon $\varepsilon Hf_{(t)}$ values from the Coast Mountains batholith typically range from +15 to +5 (Cecil et al., 2011).

Source regions that display a more evolved component are the Idaho batholith (range −8 to −28), Laramide porphyry copper province (range 0 to −23), and the Transverse Ranges (range −5 to −20). Data from the Idaho batholith (Gaschnig et al., 2011) form a consistent negative trend in $\varepsilon Hf_{(t)}$ space, ranging from −8 to −18 at ca. 85 Ma and decreasing steadily in εHf to a range of −17 to −28 from ca. 65 to 56 Ma. This is because the batholith is composed of multiple discrete bodies of peraluminous granite hosted entirely in Precambrian crust (Armstrong et al., 1977; Hyndman, 1983).

PALEOGEOGRAPHIC IMPLICATIONS

Linking the Coast Mountains Batholith and Gulf of Mexico

The paleogeography of Cretaceous through Eocene strata preserved in the Four Corners region of the Colorado Plateau, including the San Juan Basin, is well understood from a combination of paleocurrent indicators (Fassett and Hinds, 1971; Powell, 1972; Fassett, 1985; Lehman, 1985; Klute, 1986; Sikkink, 1987; Smith, 1988; Cather, 2004; Cather et al., 2012; Dickinson et al., 2012), paleoshoreline migration (Cumella, 1983; Molenaar, 1983; Hunt, 1984; Hunt and Lucas, 1992), and U-Pb ages of detrital zircons (Dickinson and Gehrels, 2008; Dickinson et al., 2010, 2012; Bush et al., 2016; Pecha et al., 2018). Our new Hf data from the San Juan Basin support earlier paleogeographic reconstructions previously outlined in Donahue (2016) and Pecha et al. (2018), and the composite of our San Juan Basin results now provides a proxy for Cretaceous and Paleocene sedimentary cover that once blanketed the Four Corners region prior to Cenozoic beveling.

Samples GOM-46 and GOM-76 were collected in west-central Arkansas near the western margin of the Mississippi embayment (Blum and Pecha, 2014; Blum et al., 2017). Blum et al. (2017) interpreted these samples to represent deposition within the ancestral Arkansas River, which has sedimentary provenance ties to the central Laramide Rockies, including the paleo–Platte River, which has provenance ties to the Sevier fold-and-thrust belt as far north as the Idaho batholith (Blum et al.,

2017). Based on initial reconstructions from Flores (2003) and Jacobson et al. (2011), the paleo–Platte River drainage extended westward beyond the Sevier fold-and-thrust belt to the drainage divide in west-central Nevada (Blum et al., 2017). The headwaters of the paleo–Platte River drainage basin also included the California River of Davis et al. (2010) and the Idaho River of Chetel et al. (2011). These notions are all supported with our new isotopic data; however, the additional presence of zircons with a more juvenile signature ($\varepsilon Hf_{[t]}$ ranging from +13 to +3) indicates additional input from outside the Laramide Rockies or the Idaho batholith (Fig. 11).

Based on our $\varepsilon Hf_{(t)}$ comparisons, only the North Cascades Range and the Coast Mountains batholith are potential matches for isotopically juvenile zircons found in the Paleocene Gulf of Mexico sediments. However, the Gulf of Mexico $\varepsilon Hf_{(t)}$ signature is composed of two distinct $\varepsilon Hf_{(t)}$ ranges: (1) from 230 to 190 Ma

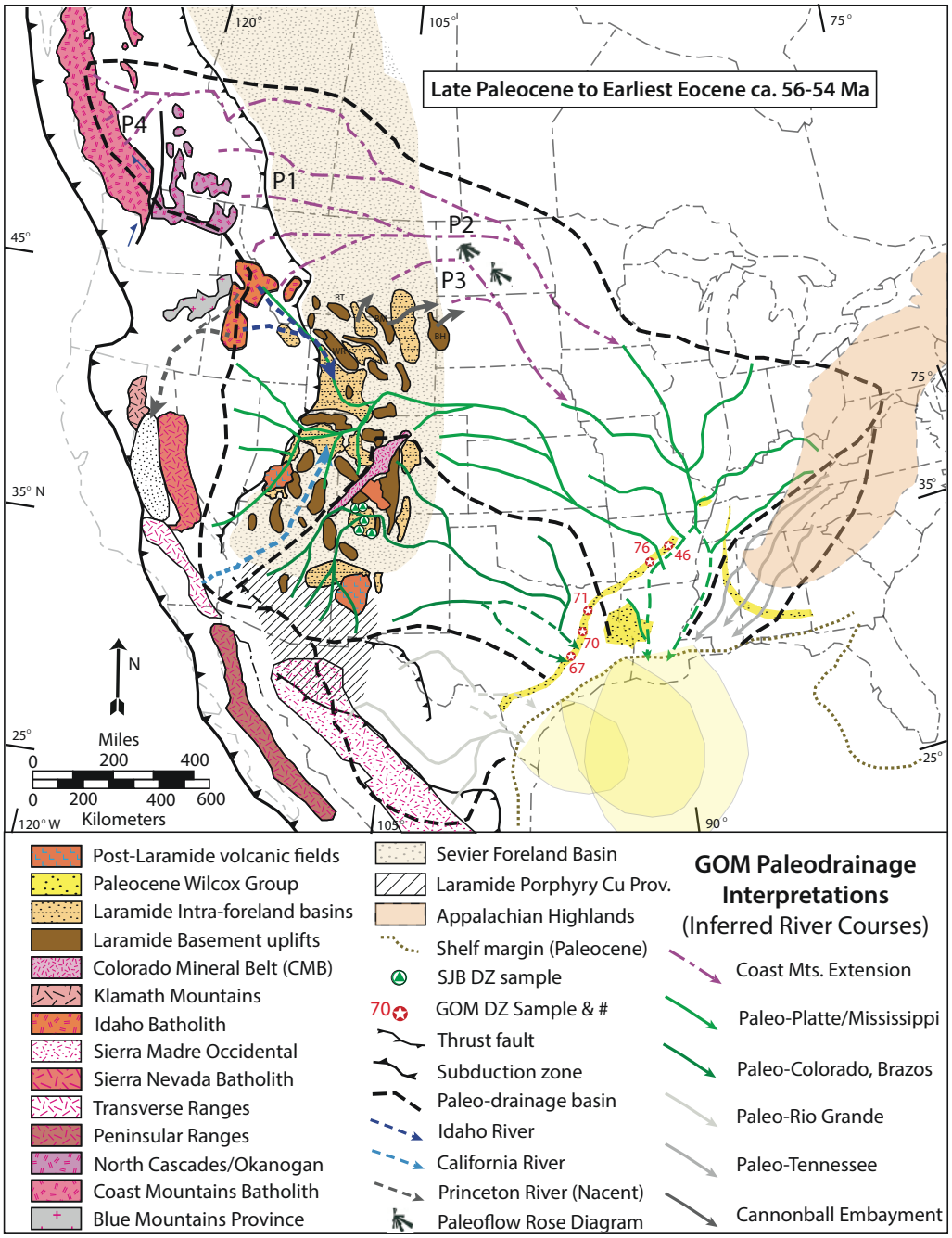

Figure 11. Paleodrainage reconstruction for the northern Gulf of Mexico (GOM) during late Paleocene to earliest Eocene Wilcox Group deposition. Inferred river courses (schematic) and interpreted drainage area boundaries are based on Blum et al. (2017), except for the modification of the paleo–Platte River and proposed increase in basin-floor fan length scale supported by this study. Rosita, Rockdale, and Holly Springs depocenters are after Fisher and McGowen (1969), Edwards (1981), and Galloway et al. (2011), and predicted slope and basin-floor fan are after Blum et al. (2017). Idaho River is from Chetel et al. (2011). Princeton River is from Dumitru et al. (2013). California River is from Davis et al. (2010). Paleoflow references are as follows: P1—post-Wapiabi Sandstone (Mack and Jerzykiewicz, 1989), P2—Sentinel Butte Formation (Daly et al., 1985), P3—Ludlow Member Fort Union Formation (Belt et al., 1984), P4—Late Cretaceous and Paleocene (Tribe, 2005). SJB—San Juan Basin; DZ—detrital zircon. BH—Black Hills; BM—Bighorn Mountains; BT—Beartooth Mountains; WR—Wind River Range.

with $\varepsilon Hf_{(t)}$ = +13 to +7, and (2) from ca. 180 to 54 Ma with $\varepsilon Hf_{(t)}$ = +15 to −1. Only the Coast Mountains batholith (Fig. 9A) can account for both contributions. The North Cascades Range only matches well with the Gulf of Mexico juvenile signature from ca. 190 to 130 Ma with $\varepsilon Hf_{(t)}$ = +15 to +5, and from ca. 130 to 100 Ma with $\varepsilon Hf_{(t)}$ = +13 to +5 (Fig. 9B). The North Cascades Range cannot account for the ca. 230–190 Ma juvenile zircons. Therefore, we propose that the Coast Mountains batholith is the probable source for the juvenile zircons deposited in the Wilcox Group during latest Paleocene to earliest Eocene time.

Three possible scenarios exist for transporting zircons from the Coast Mountains batholith to the Gulf of Mexico: (1) Zircons were transported through the air by volcanic eruptions (herein referred to as air-fall zircons), (2) hinterland river(s) tapped the Coast Mountains batholith and flowed generally south and then east and entered the paleo–Platte River drainage network, and (3) transverse river(s) originating in the Coast Mountains batholith exited the hinterland, crossed the foreland basin, and flowed all the way to the Gulf of Mexico through the paleo–Mississippi River.

To establish detrital zircon provenance, we examined each of these three scenarios. Regarding air-fall zircons, grains near depositional age (ca. 58–54 Ma) in the Gulf of Mexico samples have a unique juvenile isotopic signature ($\varepsilon Hf_{[t]}$ = +13 to 0) that only matches the Coast Mountains batholith, making this scenario plausible (Fig. 9A). However, without continuous reworking throughout the entirety of Mesozoic time, air-fall zircons cannot account for the entire age range (ca. 230–54 Ma) of juvenile zircons found in the Wilcox Group. Therefore, air-fall zircons are likely present in Wilcox Group sediments, but they only account for a very small percentage of the total flux.

Hinterland river(s) that originated in the Coast Mountains batholith and flowed southward through the hinterland seem highly unlikely. The river(s) would have had to gain elevation to climb over the Cordillera and then take an eastward passage across the thrust belt. The presence of the Princeton River (Dumitru et al., 2013) with paleoflow directed to the southwest also limits any possibilities for a southward-flowing hinterland river. However, the existence of the Salt Lake reentrant north of the Uintas or the Idaho River (Chetel et al., 2011; with later modification by Malone et al., 2014, and Craddock et al., 2015) does provide a potential exit through the thrust belt, but routing a large river to these areas is not feasible. Moreover, the Idaho River likely did not exist as such until after ca. 50 Ma, as late Paleocene and early Eocene drainage left the central Rocky Mountains to the north through the Bighorn and Powder River Basins (Welch et al., this volume). During our evaluation, we also considered the possibility of a river flowing southward immediately once it reached the foredeep in the Sevier foreland basin, paralleling the Sevier thrust front until it was captured by the Idaho River and entered the Green River basin en route to the Gulf of Mexico. However, extensive disruption of the foreland basin in western Montana and Wyoming by large elevated mountain ranges (e.g., Teton–Gros Ventre–Wind River, Beartooth, Bighorn, Tobacco Root, etc.) during the Laramide orogeny (Carrapa et al., 2019) likely prohibited a large-scale river(s) from crossing the region, without taking a highly circuitous and improbable route. The Paleogene topography of the northern Rocky Mountains region near the Idaho and Boulder batholiths (Schwartz and Schwartz, 2013; Carrapa et al., 2019; Schwartz et al., 2019) also makes it infeasible to simply extend the Idaho River to capture North Cascades and/or Coast Mountains batholith detritus, so this option is not considered further.

Numerous lines of evidence support the notion of transverse drainages flowing from the Coast Mountains batholith, exiting the thrust front, and flowing across the Great Plains region en route to the Gulf of Mexico. Tribe (2005) established that paleoflow off the eastern margin of the Coast Mountains batholith was generally toward the east-northeast, with rivers crossing the hinterland in British Columbia. In the Alberta foreland, paleocurrent indicators from late Campanian to early Paleocene sandstones (post-Wapiabi Sandstone) are generally toward the east (Mack and Jerzykiewicz, 1989), supporting the idea that these transverse rivers exited the Sevier thrust front in southern Alberta, Canada. Supporting evidence for transverse rivers draining elevated regions comes from Miall (2006) and Burbank (1992), who have shown that thrust-belt drainage systems commonly consist of a set of transverse drainages that transport eroded detritus from the orogenic highlands across the hinterland and into the foreland basin system. In the northern Great Plains region, the paleocurrents generally turn southeasterly, as evidenced by the Sentinel Butte Formation (Daly et al., 1985) and the Ludlow Member of the Fort Union Formation (Belt et al., 1984), both supporting the possibility of a transcontinent sediment pathway.

Based on the supporting evidence, we propose an extension (which we call the "Coast Mountains River") to the paleo–Mississippi River drainage basin of Galloway et al. (2011) and Blum et al. (2017) (Fig. 11), a drainage pattern that developed during latest Cretaceous time (Potter-McIntire et al., 2018). This extension extends the originally defined headwaters of the paleo–Mississippi River northwesterly by an estimated 1700 km. Late Cretaceous to Cenozoic dextral strike-slip fault restorations from Wyld et al. (2006) would place the Coast Mountains batholith slightly south of its present position in coastal British Columbia (for approximate location at ca. 58–55 Ma, see Fig. 11). Our proposed extension to the paleo–Mississippi River drainage basin is required to capture the juvenile suite of zircons from the Coast Mountains batholith. The Coast Mountains River would have exited the Coast Mountains batholith by flowing generally to the east-southeast, crossing the Sevier fold-and-thrust front in Alberta, Canada, before entering the foreland basin. This drainage network likely consisted of a series of rivers that flowed across the Great Plains region and through the established paleo–Mississippi River.

The Cannonball embayment, a marine vestige of the Cretaceous Western Interior Seaway that channeled sediment toward the north and northeast from north-central Wyoming during Late Cretaceous through middle Paleocene time (Flores, 2003; Belt

et al., 2004; Slattery et al., 2015), was taken into consideration when constructing the paleoflow of the proposed Coast Mountains River. The presence of mollusk and foraminifera fossils indicates that marine deposition within the Cannonball embayment persisted into middle Paleocene time (61.6–59.2 Ma; Fox and Ross, 1942; Cvancara, 1976; Anderson et al., 2006; Boyd and Lillegraven, 2011; Slattery et al., 2015). The timing of the final withdrawal of the Cannonball Sea is poorly constrained due to the lack of preserved age-equivalent strata in the midcontinent region; however, Gulf of Mexico shoreline data suggest the Cannonball embayment was no longer a marine depocenter by latest Paleocene time (Slattery et al., 2015). Therefore, by ca. 58–56 Ma, the Cannonball Sea was no longer a physical impediment between the headwaters of the paleo–Mississippi River and the potential Coast Mountains batholith sources.

Our paleogeographic interpretations increase the drainage basin area and length scale of the paleo–Mississippi River, which hold important implications for predicting basin-floor fan scales in deep-water Gulf of Mexico areas. The relationship between the length of the longest fluvial channel and the length of the basin-floor fan has been demonstrated by Sømme et al. (2009), where the length of the basin-floor fan (L_f) is 0.1–0.5 times the length of the drainage basin (L_{db}). This method was applied by Blum et al. (2017) to the late Paleocene to earliest Eocene paleo–Mississippi River drainage (area = 2.2×10^6 km^2, with a reconstructed drainage length of 2500 km), which resulted in a predicted basin-floor fan length (L_{bff}) ranging from 250 to 1250 km ($L_{bff} = 0.1–0.5L_{db}$). Once we add the newly incorporated area and length based on our new data, the paleo–Mississippi River drainage basin area = 2.5×10^6 km^2, and the reconstructed length = 3200 km. This results in a predicted basin-floor fan length ($L_{bff} = 0.1–0.5L_{db}$) of 320–1600 km. Our low-end estimate of 320 km conforms with the measured basin-floor fan length for this drainage by Snedden et al. (2018), which measured 392 km.

CONCLUSIONS

Comparisons of our new $\varepsilon Hf_{(t)}$ isotopic results to a comprehensive compilation of Hf isotopic data from the entire North American Cordillera reveal important provenance connections and also shed light upon the crustal evolution of the North American Cordilleran magmatic arc from ca. 285 to 55 Ma. The region of the North American Cordillera that best matches both the San Juan Basin sediments and the Wilcox Group in the Gulf of Mexico sediments is the Laramide porphyry copper province of southeastern Arizona, southwestern Mexico, and southeastern California (Mohave region). While drainage capture during the late Paleocene (Sharman et al., 2017) remains one of the leading ideas for the increase in sediment flux to the Gulf of Mexico Basin, these new $\varepsilon Hf_{(t)}$ results support the notion that the sedimentary cover that once blanketed the Laramide basement uplifts was also an important contributor of detritus to the Lower Wilcox Group. Jurassic zircons (ca. 180–150 Ma) from Gulf of Mexico and San Juan Basin strata also have similar $\varepsilon Hf_{(t)}$ ratios as magmatic zircons from the Laramide porphyry copper province, ranging from −15 to −3, as exhibited by similar Late Cretaceous decreases in $\varepsilon Hf_{(t)}$ values (~−23 to −7).

A subordinate but distinctive suite of juvenile ($\varepsilon Hf_{[t]}$ = +15 to +5) detrital zircons found in Paleocene Wilcox Group sediments in the northern Gulf of Mexico supports the notion that sediments entering the Gulf of Mexico through the Mississippi embayment were derived from a more northerly routed path (paleo–Mississippi River) through the interior of the continent. These data provide evidence that the paleodrainage basins set forth by Galloway et al. (2011) and Blum et al. (2017) are robust, but the length scale of the paleo–Mississippi River drainage basin is longer than originally estimated, with headwaters originating in the Coast Mountains batholith region of British Columbia. Based on this information, we propose that a through-going river (which we call the Coast Mountains River) must have tapped hinterland sources deep in the Coast Mountains region of British Columbia and entered the foreland basin and paleo–Mississippi River drainage system en route to deposition in the Gulf of Mexico.

ACKNOWLEDGMENTS

We thank Pete DeCelles, Barbara Carrapa, and Paul Kapp for their critical discussions throughout the entire project, Dominique Giesler and Chelsi White for their assistance in acquiring the analytical data, and Dan Alberts for acquiring the scanning electron microscope images. This work was substantially improved through critical reviews by Steven Cather and Glenn Sharman. Support for this research came from ExxonMobil Upstream Research. We also recognize the National Science Foundation (NSF) for their continued support of the Arizona LaserChron Center through grant EAR-1649254. Finally, we would like to acknowledge William Dickinson for his insight into this project before he passed away, as it was his suggestion to run Hf isotopic analyses on the San Juan Basin samples as a test for differentiating source regions beyond the scope of U-Pb ages.

REFERENCES CITED

Amelin, Y., Lee, D.C., Halliday, A.N., and Pidgeon, R.T., 1999, Nature of the Earth's earliest crust from Hf isotopes in single detrital grains: Nature, v. 399, p. 252–255, https://doi.org/10.1038/20426.

Amelin, Y., Lee, D.C., and Halliday, A.N., 2000, Early-middle Archean crustal evolution deduced from Lu-Hf and U-Pb isotopic studies of single zircon grains: Geochimica et Cosmochimica Acta, v. 64, p. 4205–4225, https://doi.org/10.1016/S0016-7037(00)00493-2.

Anderson, I., Malone, D.H., and Craddock, J.P., 2019, Preliminary detrital zircon U-Pb geochronology of the Wasatch Formation, Powder River Basin, Wyoming: The Mountain Geologist, v. 56, p. 247–266, https://doi.org/10.31582/rmag.mg.56.3.247.

Anderson, L.C., Hartman, J.H., and Wesselingh, F., 2006, Close evolutionary affinities between freshwater corbulid bivalves from the Neogene of western Amazonia and Paleogene of the northern Great Plains, USA: Journal of South American Earth Sciences, v. 21, no. 1–2, p. 28-48.

Armstrong, R.L., 1968, Sevier orogenic belt in Nevada and Utah: Geological Society of America Bulletin, v. 79, p. 429–458, https://doi.org/10.1130/0016-7606(1968)79[429:SOBINA]2.0.CO;2.

Armstrong, R.L., Taubeneck, W.H., and Hales, P.O., 1977, Rb-Sr and K-Ar geochronometry of Mesozoic rocks and their Sr isotopic composition, Oregon, Washington, and Idaho: Geological Society of America Bulletin, v. 88, no. 3, p. 397–411, https://doi.org/10.1130/0016-7606(1977)88<397:RAKGOM>2.0.CO;2.

Arvizu, H.E., and Iriondo, A., 2011, Estudios isotopicos de Hf en zircons de granitoides permicos en el NW de Mexico: Evidencia de mezcla de magmas generados a partir de la fusion de multiples fuentes corticales: Revista Mexicana de Ciencias Geológicas, v. 28, p. 493–518.

Ayers, W.B., Jr., Ambrose, W.A., and Yeh, J.S., 1994, Coalbed methane in the Fruitland Formation, San Juan Basin: Depositional and structural controls on occurrence and resources, *in* Ayers, W.B., Jr., and Kaiser, W.R., eds., Coalbed Methane in the Cretaceous Fruitland Formation, San Juan Basin, New Mexico and Colorado: New Mexico Bureau of Mines and Mineral Resources Bulletin 146, p. 13–61, https://geoinfo.nmt.edu/publications/monographs/bulletins/downloads/146/Bulletin146.pdf.

Baltz, E.H., 1967, Stratigraphy and Regional Tectonic Implications of Part of Upper Cretaceous and Tertiary Rocks, East-Central San Juan Basin, New Mexico: U.S. Geological Survey Professional Paper 552, 101 p., https://doi.org/10.3133/pp552.

Barnes, H., Baltz, E.H., Jr., and Hayes, P.T., 1954, Geology and Fuel Resources of the Red Mesa Area, La Plata and Archuleta Counties, Colorado: U.S. Geologic Survey Oil and Gas Investigations Map OM-149, scale 1:62,500, https://doi.org/10.3133/om149.

Barth, A.P., Wooden, J.L., Mueller, P.A., and Economos, R.C., 2016, Granite provenance and intrusion in arcs: Evidence from diverse zircon types in Big Bear Lake Intrusive Suite, USA: Lithos, v. 246–247, p. 261–278, https://doi.org/10.1016/j.lithos.2015.12.009.

Belt, E.S., Flores, R.M., Warwick, P.D., Conway, K.M., Johnson, K.R., and Waskowitz, R.S., 1984, Relationship of fluviodeltaic facies to coal deposition in the Lower Fort Union Formation (Paleocene), south-western North Dakota, *in* Rahmani, R.A., and Flores, R.M., eds., Sedimentology of Coal and Coal-Bearing Sequences: International Association of Sedimentologists Special Publication 7, p. 177–195, https://doi.org/10.1002/9781444303797.ch10.

Belt, E.S., Hartman, J.H., Diemer, J.A., Kroeger, T.J., Tibert, N.E., and Curran, H.A., 2004, Unconformities and age relationships, Tongue River and older members of the Fort Union Formation (Paleocene), western Williston Basin, USA: Rocky Mountain Geology, v. 39, p. 113–140, https://doi.org/10.2113/39.2.113.

Bird, P., 1984, Laramide crustal thickening event in the Rocky Mountain foreland and Great Plains: Tectonics, v. 3, p. 741–758, https://doi.org/10.1029/TC003i007p00741.

Blum, M.D., and Aslan, A., 2006, Signatures of climate vs. sea-level change within incised valley-fill successions: Quaternary examples from the Texas Gulf Coast: Sedimentary Geology, v. 190, p. 177–211, https://doi.org/10.1016/j.sedgeo.2006.05.024.

Blum, M.D., and Pecha, M., 2014, Mid-Cretaceous to Paleocene North American drainage reorganization from detrital zircons: Geology, v. 42, p. 607–610, https://doi.org/10.1130/G35513.1.

Blum, M.D., and Price, D.M., 1988, Quaternary alluvial plain, *in* Shanley, K., and McCabe, P., eds., Relative Role of Eustasy, Climate, and Tectonism in Continental Rocks: Society of Economic Paleontologists and Mineralogists (SEPM) Special Publication 59, p. 31–48, https://doi.org/102110/pec.98.59.0031.

Blum, M.D., Milliken, K.T., Pecha, M.E., Snedden, J.W., Frederick, B.C., and Galloway, W.E., 2017, Detrital-zircon records of Cenomanian, Paleocene, and Oligocene Gulf of Mexico drainage integration and sediment routing: Implications for scales of basin-floor fans: Geosphere, v. 13, no. 6, p. 2169–2205, https://doi.org/10.1130/GES01410.1.

Botev, Z.I., Gortowski, J.F., and Kroese, D.P., 2010, Kernel density estimation via diffusion: Annals of Statistics, v. 38, p. 2916–2957, https://doi.org/10.1214/10-AOS799.

Bouvier, A., Vervoort, J., and Patchett, J., 2008, The Lu-Hf and Sm-Nd isotopic composition of CHUR: Constraints from unequilibrated chondrites and implications for the bulk composition of terrestrial planets: Earth and Planetary Science Letters, v. 273, p. 48–57, https://doi.org/10.1016/j.epsl.2008.06.010.

Boyd, D.W., and Lillegraven, J.A., 2011, Persistence of the Western Interior Seaway: Historical background and significance of ichnogenus Rhizocorallium in Paleocene strata, south-central Wyoming: Rocky Mountain Geology, v. 46, no. 1, p. 43–69.

Brister, B.S., and Chapin, C.E., 1994, Sedimentation and tectonics of the Laramide San Juan sag, southwestern Colorado: The Mountain Geologist, v. 31, p. 2–18.

Brown, W.G., 1988, Deformational style of Laramide uplifts in the Wyoming foreland, *in* Schmidt, C.J., and Perry, W.J., Jr., eds., Interaction of the Rocky Mountain Foreland and the Cordilleran Thrust Belt: Geological Society of America Memoir 171, p. 1–26, https://doi.org/10.1130/MEM171-p1.

Burbank, D.W., 1992, Causes of recent Himalayan uplift deduced from deposited patterns in the Ganges basin: Nature, v. 357, p. 680–683, https://doi.org/10.1038/357680a0.

Busby-Spera, C.J., Mattinson, J.M., and Schermer, E.R., 1990, The Triassic–Jurassic magmatic arc in the Mohave-Sonoran Desert and the Sierra-Klamath region: Similarities and differences in paleogeographic evolution, *in* Harwood, D.S., and Miller, M.M., eds., Paleozoic and Early Mesozoic Paleogeographic Relations: Sierra Nevada, Klamath Mountains, and Related Terranes: Geological Society of America Special Paper 255, p. 325–338, https://doi.org/10.1130/SPE255-p325.

Bush, M.A., Horton, B.K., Murphy, M.A., and Stockli, D.F., 2016, Detrital record of initial basement exhumation along the Laramide deformation front, southern Rocky Mountains: Tectonics, v. 35, p. 2117–2130, https://doi.org/10.1002/2016TC004194.

Carroll, A.R., Chetel, L.M., and Smith, M.E., 2006, Feast to famine: Sediment supply control on Laramide basin fill: Geology, v. 34, p. 197–200, https://doi.org/10.1130/G22148.1.

Carrapa, B., DeCelles, P.G., and Romero, M., 2019, Early inception of the Laramide orogeny in southwestern Montana and northern Wyoming: Implications for models of flat-slab subduction: Journal of Geophysical Research–Solid Earth, v. 124, p. 2102–2123, https://doi.org/10.1029/2018JB016888.

Cassel, E.J., Grove, M., and Graham, S.A., 2012, Eocene drainage evolution and erosion of the Sierra Nevada batholith across northern California and Nevada: American Journal of Science, v. 312, p. 117–144, https://doi.org/10.2475/02.2012.03.

Cather, S.M., 2003, Polyphase Laramide tectonism and sedimentation in the San Juan Basin, New Mexico, *in* Lucas, S.G., Semken, S.C., Berglof, W.R., and Ulmer-Scholle, D.S., eds., Geology of the Zuni Plateau: Socorro, New Mexico, New Mexico Geological Society, 54th Field Conference Guidebook, p. 119–132.

Cather, S.M., 2004, Laramide orogeny in central and northern New Mexico and southern Colorado, *in* Mack, G.H., and Giles, K.A., eds., The Geology of New Mexico; A Geologic History: Socorro, New Mexico, New Mexico Geological Society, p. 203–248.

Cather, S.M., Chapin, C.E., and Kelley, S.A., 2012, Diachronous episodes of Cenozoic erosion in southwestern North America and their relationship to surface uplift, paleoclimate, paleodrainage, and paleoaltimetry: Geosphere, v. 8, p. 1177–1206, https://doi.org/10.1130/GES00801.1.

Cather, S.M., Heizler, M.T., and Williamson, T.E., 2019, Laramide fluvial evolution of the San Juan Basin, New Mexico and Colorado: Paleocurrent and detrital-sanidine age constraints from the Paleocene Nacimiento and Animas formations: Geosphere, v. 15, p. 1641–1664, https://doi.org/10.1130/GES02072.1.

Cecil, M.R., Gehrels, G.E., Ducea, M.N., and Patchett, P.J., 2011, U-Pb–Hf characterization of the central Coast Mountains batholith: Implications for petrogenesis and crustal architecture: Lithosphere, v. 3, p. 247–260, https://doi.org/10.1130/L134.1.

Chapman, J.B., Dafov, M.N., Gehrels, G., Ducea, M.N., Valley, J.W., and Ishida, A., 2018, Lithospheric architecture and tectonic evolution of the southwestern U.S. Cordillera: Constraints from zircon Hf and O isotopic data: Geological Society of America Bulletin, v. 130, p. 2031–2046, https://doi.org/10.1130/B31937.1.

Chetel, L.M., Janecke, S.U., Carroll, A.R., Beard, B.L., Johnson, C.M., and Singer, B.S., 2011, Paleogeographic reconstruction of the Eocene Idaho River, North American Cordillera: Geological Society of America Bulletin, v. 123, p. 71–88, https://doi.org/10.1130/B30213.1.

Coney, P.J., and Reynolds, S.J., 1977, Cordilleran Benioff zone: Nature, v. 270, p. 403–406, https://doi.org/10.1038/270403a0.

Constenius, K.N., Esser, R.P., and Layer, P.W., 2003, Extensional collapse of the Charleston-Nebo salient and its relationship to space-time variations in Cordilleran orogenic belt tectonism and continental stratigraphy, *in* Raynolds, R.G., and Flores, R.M., eds., Cenozoic Systems of the Rocky Mountain Region: Denver, Colorado, Rocky Mountain Section, Society for Sedimentary Geology (SEPM), p. 303–353.

Craddock. J.P., Malone, D.H., Porter, R., MacNamee, A.F, Mathisen, M., Leonard, A.M., and Kravits, K., 2015, Structure, timing, and kinematics of the early Eocene South Fork Slide, northwest Wyoming, USA: Journal of Geology, v. 123, p. 311–335, https://doi.org/10.1086/682288.

Craddock, J.P., Malone, D.H., Konstantinou, A., Spruell, J., and Porter, R., 2022, this volume, Calcite twinning strains associated with Laramide uplifts, Wyoming Province, *in* Craddock, J.P., Malone, D.H., Foreman, B.Z., and Konstantinou, A., eds., Tectonic Evolution of the Sevier-Laramide Hinterland, Thrust Belt, and Foreland, and Postorogenic Slab Rollback (180–20 Ma): Geological Society of America Special Paper 555, Chapter 6, https://doi.org/10.1130/2021.2555(06).

Craigg, S.D., 2001, Geologic Framework of the San Juan Structural Basin of New Mexico, Colorado, Arizona, and Utah with Emphasis on Triassic through Tertiary Rocks: U.S. Geological Survey Professional Paper 1420, 70 p., https://pubs.usgs.gov/pp/1420/report.pdf.

Cumella, S.P., 1983, Relation of Upper Cretaceous regressive sandstone units of the San Juan Basin to source area tectonics, *in* Reynolds, M.W., and Dolly, E.D., eds., Mesozoic Paleogeography of West-Central United States: Denver, Colorado, Rocky Mountain Section, Society for Sedimentary Geology (SEPM), p. 189–199.

Cvancara, A.M., 1976, Geology of the Cannonball Formation (Paleocene) in the Williston Basin, With Reference to Uranium Potential: North Dakota Geological Survey Report of Investigation No. 57 (No. GJO-1633-3), 22 p. + plates, https://www.osti.gov/biblio/7341755.

Dafov, M.N., Carrera, A., Gehrels, G.E., Alberst, D., Pereira, M., Cecil, M.R., Rusmore, M.E., Stowell, H.H., and Woodsworth, G.J., 2020, U-Th-Pb geochronology and Lu-Hf isotope geochemistry of detrital zircons in metasedimentary rocks of the southern Coast Mountains batholith: Lithosphere, v. 2020, 8854686, https://doi.org/10.2113/2020/8854686.

Daly, D.J., Groenewold, G.H., and Schmit, C.R., 1985, Paleoenvironments of the Paleocene Sentinel Butte Formation, Knife River area, west-central North Dakota, *in* Flores, R.M., and Kaplan, S.S., eds., Cenozoic Paleogeography of the West-Central United States: Denver, Colorado, Rocky Mountain Section, Society for Sedimentary Geology (SEPM), p. 171–185.

Davis, S.J., Mulch, A., Carroll, A.R., Horton, T.W., and Chamberlain, C.P., 2009, Paleogene landscape evolution of the central North American Cordillera: Developing topography and hydrology in the Laramide foreland: Geological Society of America Bulletin, v. 121, p. 100–116, https://doi.org/10.1130/B26308.1.

Davis, S.J., Dickinson, W.R., Gehrels, G.E., Spencer, J.E., Lawton, T.F., and Carroll, A.R., 2010, The Paleogene California River: Evidence of Mojave-Uinta paleodrainage from U-Pb ages of detrital zircons: Geology, v. 38, p. 931–934, https://doi.org/10.1130/G31250.1.

DeCelles, P.G., 2004, Late Jurassic to Eocene evolution of the Cordilleran thrust belt and foreland basin system, western U.S.: American Journal of Science, v. 304, p. 105–168, https://doi.org/10.2475/ajs.304.2.105.

DeCelles, P.G., Gray, M.B., Ridgway, K.D., Cole, R.B., Srivastava, P., Pequera, N., and Pivnik, D.A., 1991, Kinematic history of foreland uplift from Paleocene synorogenic conglomerate, Beartooth Range, Wyoming and Montana: Geological Society of America Bulletin, v. 103, p. 1458–1475, https://doi.org/10.1130/0016-7606(1991)103<1458:KHOAFU>2.3.CO;2.

Dickinson, W.R., 2000, Geodynamic interpretation of Paleozoic tectonic trends oriented oblique to the Mesozoic Klamath-Sierran continental margin in California, *in* Soreghan, M.J., and Gehrels, G.E., eds., Paleozoic and Triassic Paleogeography and Tectonics of Western Nevada and Northern California: Geological Society of America Special Paper 347, p. 209–245, https://doi.org/10.1130/0-8137-2347-7.209.

Dickinson, W.R., 2004, Evolution of the North American Cordillera: Annual Review of Earth and Planetary Sciences, v. 32, p. 13–45, https://doi.org/10.1146/annurev.earth.32.101802.120257.

Dickinson, W.R., and Gehrels, G.E., 2008, Sediment delivery to the Cordilleran foreland basin: Insights from U-Pb ages of detrital zircons in Upper Jurassic and Cretaceous strata of the Colorado Plateau: American Journal of Science, v. 308, p. 1041–1082, https://doi.org/10.2475/10.2008.01.

Dickinson, W.R., and Lawton, T.F., 2001a, Carboniferous to Cretaceous assembly and fragmentation of Mexico: Geological Society of America Bulletin, v. 113, p. 1142–1160, https://doi.org/10.1130/0016-7606(2001)113<1142:CTCAAF>2.0.CO;2.

Dickinson, W.R., and Lawton, T.F., 2001b, Tectonic setting and sandstone petrofacies of the Bisbee basin (USA-Mexico): Journal of South American Earth Sciences, v. 14, p. 475–504, https://doi.org/10.1016/S0895-9811(01)00046-3.

Dickinson, W.R., and Snyder, W.S., 1978, Plate tectonics of the Laramide orogeny, *in* Matthews, V., ed., Laramide Folding Associated with Basement Block Faulting in the Western United States: Geological Society of America Memoir 151, p. 355–366, https://doi.org/10.1130/MEM151-p355.

Dickinson, W.R., Klute, M.A., Hayes, M.J., Janecke, S.U., Lundin, E.R., McKittrick, M.A., and Olivares, M.D., 1988, Paleogeographic and paleotectonic setting of Laramide sedimentary basins in the central Rocky Mountain region: Geological Society of America Bulletin, v. 100, p. 1023–1039, https://doi.org/10.1130/0016-7606(1988)100<1023:PAPSOL>2.3.CO;2.

Dickinson, W.R., Cather, S.M., and Gehrels, G.E., 2010, Detrital zircon evidence for derivation of arkosic sand in eolian Narbona Pass Member of the Eocene–Oligocene Chuska Sandstone from Precambrian basement rocks in central Arizona, *in* Fassett, J.E., et al., eds., Geology of the Four Corners Country: Socorro, New Mexico, New Mexico Geological Society, 61st Annual Field Conference Guidebook, p. 125–134.

Dickinson, W.R., Lawton, T.F., Pecha, M., Davis, S.J., Gehrels, G.E., and Young, R.A., 2012, Provenance of the Paleogene Colton Formation (Uinta Basin) and Cretaceous–Paleogene provenance evolution in the Utah foreland: Evidence from U-Pb ages of detrital zircons, paleocurrent trends, and sandstone petrofacies: Geosphere, v. 8, p. 854–880, https://doi.org/10.1130/GES00763.1.

Donahue, M.M., 2016, Episodic Uplift of the Rocky Mountains: Evidence from U-Pb Detrital Zircon Geochronology and Low-Temperature Thermochronology with a Chapter on Using Mobile Technology for Geoscience Education [Ph.D. dissertation]: Albuquerque, New Mexico, University of New Mexico, UNM Digital Repository, 1177 p.

Dumitru, T.A., Ernst, W.G., Wright, J.E., Wooden, J.L., Wells, R.E., Farmer, L.P., Kent, A.J.R., and Graham, S.A., 2013, Eocene extension in Idaho generated massive sediment floods into the Franciscan trench and into the Tyee, Great Valley, and Green River basins: Geology, v. 41, p. 187–190, https://doi.org/10.1130/G33746.1.

Edwards, M.B., 1981, Upper Wilcox Rosita delta system of south Texas: Growth-faulted shelf-edge deltas: American Association of Petroleum Geologists Bulletin, v. 65, p. 54–73, https://doi.org/10.1306/2F91976F-16CE-11D7-8645000102C1865D.

Elston, D.P., and Young, R.A., 1991, Cretaceous–Eocene (Laramide) landscape development and Oligocene–Pliocene drainage reorganization of Transition Zone and Colorado Plateau, Arizona: Journal of Geophysical Research, v. 96, p. 12,389–12,406, https://doi.org/10.1029/90JB01978.

English, J.M., Johnston, S.T., and Wang, K., 2003, Thermal modeling of the Laramide orogeny: Testing the flat-slab subduction hypothesis: Earth and Planetary Science Letters, v. 214, p. 619–632, https://doi.org/10.1016/S0012-821X(03)00399-6.

Epis, R.C., and Chapin, C.E., 1975, Geomorphic and tectonic implications of the post-Laramide, late Eocene erosion surface in the southern Rocky Mountains, *in* Curtis, B.F., ed., Cenozoic History of the Southern Rocky Mountains: Geological Society of America Memoir 144, p. 45–74, https://doi.org/10.1130/MEM144-p45.

Ewing, T.E., and Galloway, W.E., 2019, Evolution of the northern Gulf of Mexico Sedimentary Basin, *in* Miall, A., ed., The Sedimentary Basins of the United States and Canada (2nd ed.): Amsterdam, Elsevier, p. 627–694, https://doi.org/10.1016/B978-0-444-63895-3.00016-4.

Fassett, J.E., 1985, Early Tertiary paleogeography and paleotectonics of the San Juan Basin area, New Mexico and Colorado, *in* Flores, R.M., and Kaplan, S.S., eds., Cenozoic Paleogeography of the West-Central United States: Denver, Colorado, Rocky Mountain Section, Society of Economic Paleontologists and Mineralogists (SEPM), p. 317–334.

Fassett, J.E., and Hinds, J.S., 1971, Geology and Fuel Resources of the Fruitland Formation and Kirtland Shale of the San Juan Basin, New Mexico and Colorado: U.S. Geological Survey Professional Paper 676, 76 p., https://doi.org/10.3133/pp676.

Finzel, E.S., 2017, Detrital zircon microtextures and U-Pb geochronology of Upper Jurassic to Paleocene strata in the distal North American Cordillera foreland basin: Tectonics, v. 36, no. 7, p. 1295–1316, https://doi.org/10.1002/2017TC004549.

Fisher, C.M., Hanchar, J.M., Miller, C.F., Phillips, S., Vervoort, J.D., and Whitehouse, M.J., 2017, Combining Nd isotopes in monazite and Hf isotopes in zircon to understand complex open-system processes in granitic magmas: Geology, v. 45, p. 267–270, https://doi.org/10.1130/G38458.1.

Fisher, W.L., and McGowen, J.H., 1969, Depositional systems in Wilcox Group (Eocene) of Texas and their relation to occurrence of oil and gas:

American Association of Petroleum Geologists Bulletin, v. 53, p. 30–54, https://doi.org/10.1306/5D25C591-16C1-11D7-8645000102C1865D.

Flores, R.M., 2003, Paleocene paleogeographic, paleotectonic, and paleoclimatic patterns of the northern Rocky Mountains and Great Plains region, *in* Raynolds, R.G., and Flores, R.M., eds., Cenozoic Systems of the Rocky Mountain Region: Denver, Colorado, Rocky Mountain Section, Society for Sedimentary Geology (SEPM), p. 63–106.

Foreman, B.Z., D'Emic, M.D., Malone, D., and Craddock, J., 2022, this volume, Over- to under- to back-filled: Early evolution of the Sevier Foreland Basin in Wyoming, USA, *in* Craddock, J.P., Malone, D.H., Foreman, B.Z., and Konstantinou, A., eds., Tectonic Evolution of the Sevier-Laramide Hinterland, Thrust Belt, and Foreland, and Postorogenic Slab Rollback (180–20 Ma): Geological Society of America Special Paper 555, Chapter 3, https://doi.org/10.1130/2021.2555(03).

Fox, S.K., Jr., and Ross, R.J., Jr., 1942, Foraminiferal evidence for the Midway (Paleocene) age of the Cannonball Formation in North Dakota: Journal of Paleontology, v. 16, no. 5, p. 660–673, https://www.jstor.org/stable/1298789.

Galloway, W.E., 2005, Gulf of Mexico Basin depositional record of Cenozoic North American drainage basin evolution, *in* Blum, M.D., Marriott, S.B., and Leclair, S.F., eds., Fluvial Sedimentology VII: International Association of Sedimentologists Special Publication 35, p. 409–423, https://doi.org/10.1002/9781444304350.ch22.

Galloway, W.E., 2008, Depositional evolution of the Gulf of Mexico sedimentary basin, *in* Miall, A.D., ed., Sedimentary Basins of the World, Volume 5: The Sedimentary Basins of the United States and Canada: Amsterdam, Elsevier, p. 505–549, https://doi.org/10.1016/S1874-5997(08)00015-4.

Galloway, W.E., Ganey-Curry, P.E., Li, X., and Buffler, R.T., 2000, Cenozoic depositional history of the Gulf of Mexico Basin: American Association of Petroleum Geologists Bulletin, v. 84, p. 1743–1774, https://doi.org/10.1306/8626C37F-173B-11D7-8645000102C1865D.

Galloway, W.E., Whiteaker, T.L., and Ganey-Curry, P., 2011, History of Cenozoic North American drainage basin evolution, sediment yield, and accumulation in the Gulf of Mexico Basin: Geosphere, v. 7, p. 938–973, https://doi.org/10.1130/GES00647.1.

Garcia, J.A., Mahar, M.A., Goodell, P.C., Molina, C., and Ricketts, J.W., 2021, Petrology, geochemistry, stratigraphy, zircon U-Pb geochronology and Hf isotopic compositions of subsurface lithologies in northwestern Mesa Central, Durango, Mexico: Implications for the tectonomagmatic evolution of northwestern Mexico: Gondwana Research, v. 93, p. 1–25, https://doi.org/10.1016/j.gr.2021.01.005.

Gaschnig, R.M., Vervoort, J.D., Lewis, R.S., and Tikoff, B., 2011, Isotopic evolution of the Idaho batholith and Challis intrusive province, northern US Cordillera: Journal of Petrology, v. 52, p. 2397–2429, https://doi.org/10.1093/petrology/egr050.

Gehrels, G.E., 2012, Detrital zircon U-Pb geochronology: Current methods and new opportunities, *in* Busby, C., and Azor, A., eds., Tectonics of Sedimentary Basins: Recent Advances: Oxford, UK, Blackwell Publishing Ltd., p. 45–62, https://doi.org/10.1002/9781444347166.ch2.

Gehrels, G., and Pecha, M., 2014, Detrital zircon U-Pb geochronology and Hf isotope geochemistry of Paleozoic and Triassic passive margin strata of western North America: Geosphere, v. 10, p. 49–65, https://doi.org/10.1130/GES00889.1.

Giesler, D., Gehrels, G., Pecha, M., White, C., Yokelson, I., and McClelland, W., 2016, U-Pb and Hf isotopic analysis of detrital zircons from the Taku terrane, southeast Alaska: Canadian Journal of Earth Sciences, v. 53, p. 979–992, https://doi.org/10.1139/cjes-2015-0240.

Gonzales, D.A., 2010, The enigmatic Late Cretaceous McDermott Formation, *in* Fassett, J.E., et al., eds., Geology of the Four Corners Country: Socorro, New Mexico, New Mexico Geological Society, 61st Annual Field Conference Guidebook, p. 157–162.

Gonzales, D.A., 2015, New U-Pb zircon and $^{40}Ar/^{39}Ar$ age constraints on the late Mesozoic to Cenozoic plutonic record in the western San Juan Mountains: The Mountain Geologist, v. 52, p. 5–42.

Gorham, T.W., and Ingersoll, R.V., 1979, Evolution of the Eocene Galisteo basin, north-central New Mexico, *in* Ingersoll, R.V., Woodward, L.A., and James, H.L., eds., Santa Fe Country: Socorro, New Mexico, New Mexico Geological Society, 30th Field Conference Guidebook, p. 219–224.

Hamlin, H.S., 1988, Depositional and Ground-Water Flow Systems of the Carizzo–Upper Wilcox, South Texas: Bureau of Economic Geology, The University of Texas at Austin, Report of Investigations 175, 61 p.

Henry, C.D., 2008, Ash-flow tuffs and paleovalleys in northeastern Nevada: Implications for Eocene paleogeography and extension in the Sevier hinterland, northern Great Basin: Geosphere, v. 4, p. 1–35, https://doi.org/10.1130/GES00122.1.

Homan, E., 2017, Investigating Causes of Magmatic Episodicity in the Southern Coast Mountains Batholith, British Columbia: Insights from Hafnium and Oxygen Isotopes in Magmatic Zircon [Ph.D. thesis]: Northridge, California State University, 128 p.

Hunt, A.P., 1984, Stratigraphy, Sedimentology, Taphonomy and Magnetostratigraphy of the Fossil Forest Area, San Juan County, New Mexico [M.S. thesis]: Socorro, New Mexico, New Mexico Institute of Mining and Technology, 338 p.

Hunt, A.P., and Lucas, S.G., 1992, Stratigraphy, paleontology and age of the Fruitland and Kirtland Formations (Upper Cretaceous), San Juan Basin, New Mexico, *in* Lucas, S.G., Kues, B.S., Williamson, T.E., and Hunt, A.P., eds., San Juan Basin IV: Socorro, New Mexico, New Mexico Geological Society, 43rd Field Conference Guidebook, p. 297–309.

Hyndman, D.W., 1983, The Idaho batholith and associated plutons, Idaho and western Montana, *in* Roddick, J.A., ed., Circum-Pacific Plutonic Terranes: Geological Society of America Memoir 159, p. 213–240, https://doi.org/10.1130/MEM159-p213.

Jackson, W.T., Jr., McKay, M.P., Beebe, D.A., Mullins, C., Ionescu, A., Shaulis, B., and Barbeau, D.L., 2021, Late Cretaceous sediment provenance in the eastern Gulf Coastal Plain (USA) based on detrital-zircon U-Pb ages and Th/U values: Journal of Sedimentary Research, v. 91, no. 10, p. 1025–1039, https://doi.org/10.2110/jsr.2020.177.

Jacobson, C.E., Grove, M., Pedrick, J.N., Barth, A.P., Marsaglia, K.M., Gehrels, G.E., and Nourse, J.A., 2011, Late Cretaceous–early Cenozoic tectonic evolution of the southern California margin inferred from provenance of trench and forearc sediments: Geological Society of America Bulletin, v. 123, p. 485–506, https://doi.org/10.1130/B30238.1.

Jordan, T.E., 1981, Thrust loads and foreland basin evolution, Cretaceous, western United States: American Association of Petroleum Geologists Bulletin, v. 65, p. 2506–2520, https://doi.org/10.1306/03B599F4-16D1-11D7-8645000102C1865D.

Kelley, V.C., 1950, Precambrian rocks of the San Juan Basin, *in* Guidebook of the San Juan Basin, New Mexico and Arizona: Socorro, New Mexico, New Mexico Geological Society, 1st Field Conference Guidebook, p. 53–55.

Kelley, V.C., 1951, Tectonics of the San Juan Basin: Socorro, New Mexico, New Mexico Geological Society, 2nd Field Conference Guidebook, p. 124–131.

Klute, M.A., 1986, Sedimentology and sandstone petrography of the upper Kirtland Shale and Ojo Alamo Sandstone, Cretaceous–Tertiary boundary, western and southern San Juan Basin, New Mexico: American Journal of Science, v. 286, p. 463–488, https://doi.org/10.2475/ajs.286.6.463.

Kottlowski, F.E., 1957, Mesozoic strata flanking the southwestern San Juan Mountains, Colorado and New Mexico, *in* Kottlowski, F.E., and Baldwin, B., eds., Southwestern San Juan Mountains (Colorado): Socorro, New Mexico, New Mexico Geological Society, 8th Field Conference Guidebook, p. 138–153.

Lackey, J.S., Cecil, M.R., Cameron, J.W., Bindeman, I.N., and Gehrels, G.E., 2012, The Fine Gold intrusive suite: The roles of basement terranes and magma source development in the Early Cretaceous Sierra Nevada batholith: Geosphere, v. 8, p. 292–313, https://doi.org/10.1130/GES00745.1.

Laskowski, A.K., DeCelles, P.G., and Gehrels, G.E., 2013, Detrital zircon geochronology of Cordilleran retroarc foreland basin strata, western North America: Tectonics, v. 32, no. 5, p. 1027–1048, https://doi.org/10.1002/tect.20065.

Lawton, T.F., 2004, Upper Jurassic and Lower Cretaceous strata of southwestern New Mexico and northern Chihuahua, Mexico, *in* Mack, G.H., and Giles, K.A., eds., The Geology of New Mexico; A Geologic History: New Mexico Geological Society Special Publication 11, p. 153–168.

Lawton, T.F., 2008, Laramide sedimentary basins, *in* Miall, A.D., ed., Sedimentary Basins of the World, Volume 5: The Sedimentary Basins of the United States and Canada: Amsterdam, Elsevier, p. 429–450, https://doi.org/10.1016/S1874-5997(08)00012-9.

Lawton, T.F., 2019, Laramide sedimentary basins and sediment-dispersal systems, *in* Miall, A., The Sedimentary Basins of the United States and Canada (2nd ed.): Amsterdam, Elsevier, p. 529–557, https://doi.org/10.1016/B978-0-444-63895-3.00013-9.

Lawton, T.F., and Bradford, B.A., 2011, Correlation and provenance of Upper Cretaceous (Campanian) fluvial strata in the Cordilleran foreland basin, Utah, from zircon U-Pb geochronology and petrography: Journal of Sedimentary Research, v. 81, p. 495–512, https://doi.org/10.2110/jsr.2011.45.

Lazear, G., Karlstrom, K.E., Aslan, A., and Kelley, S., 2013, Denudation and flexural isostatic response of the Colorado Plateau and southern Rocky Mountain region since 10 Ma: Geosphere, v. 9, p. 792–814, https://doi.org/10.1130 /GES00836. 1.

Lechler, A.R., and Niemi, N.A., 2011, Sedimentologic and isotopic constraints on the Paleogene paleogeography and paleotopography of the southern Sierra Nevada, California: Geology, v. 39, p. 379–382, https://doi.org/10.1130/G31535.1.

Lehman, T.M., 1985, Depositional environments of the Naashoibito Member of the Kirtland Shale, Upper Cretaceous, San Juan Basin, New Mexico, *in* Wolberg, D.L., compiler, Contributions to Late Cretaceous Paleontology and Stratigraphy of New Mexico: New Mexico Bureau of Mines and Mineral Resources Circular 195, p. 55–79, https://geoinfo.nmt.edu/publications/monographs/circulars/downloads/195/Circular-195.pdf.

Leveille, R.A., and Stegen, R.J., 2012, The southwestern North America porphyry copper province, *in* Hedenquist, J.W., Harris, M., and Camus, F., eds., Geology and Genesis of Major Copper Deposits and Districts of the World: A Tribute to Richard H. Sillitoe: Society of Economic Geologists Special Publication 16, p. 361–401, https://doi.org/10.5382/SP.16.15.

Liu, L., Gurnis, M., Seton, M., Saleeby, J., Muller, R.D., and Jackson, J.M., 2010, The role of oceanic plateau subduction in the Laramide orogeny: Nature Geoscience, v. 3, p. 353–357, https://doi.org/10.1038/ngeo829.

Loope, D.B., and Secord, R., 2017, Interactions of a Paleocene river, a rising fold, and early-diagenetic concretions: Journal of Sedimentary Research, v. 87, no. 8, p. 866–879.

Loucks, R.G., Dodge, M.M., and Galloway, W.E., 1986, Controls on Porosity and Permeability of Hydrocarbon Reservoirs in Lower Tertiary Sandstones along the Texas Gulf Coast: The University of Texas at Austin, Bureau of Economic Geology Report of Investigations 149, 78 p.

Lowell, J.D., 1974, Plate tectonics and foreland basement deformation: Geology, v. 2, p. 275–278, https://doi.org/10.1130/0091-7613(1974)2<275:PTAFBD>2.0.CO;2.

Lucas, S.G., 2004, The Triassic and Jurassic systems in New Mexico, *in* Mack, G.H., and Giles, K.A., eds., The Geology of New Mexico; A Geologic History: New Mexico Geological Society Special Publication 11, p. 137–152.

Mack, G.H., and Jerzykiewicz, T., 1989, Detrital modes of sand and sandstone derived from andesitic rocks as a paleoclimatic indicator: Sedimentary Geology, v. 65, p. 35–44, https://doi.org/10.1016/0037-0738(89)90004-3.

Mackey, G.N., Horton, B.K., and Milliken, K.L., 2012, Provenance of the Paleocene–Eocene Wilcox Group, western Gulf of Mexico Basin: Evidence for integrated drainage of the southern Laramide Rocky Mountains and Cordilleran arc: Geological Society of America Bulletin, v. 124, p. 1007–1024, https://doi.org/10.1130/B30458.1.

Mahar, M.A., Goodell, P.C., and Feinstein, M.N., 2016, Tectono-magmatic evolution of the Chihuahua-Sinaloa border region in northern Mexico: Insights from zircon-apatite U-Pb geochronology, zircon Hf isotope composition and geochemistry of granodiorite intrusions: Lithos, v. 264, p. 555–576, https://doi.org/10.1016/j.lithos.2016.09.019.

Malone, D.H., Craddock, J.P., and Schroeder, K.A., 2014, Detrital zircon age and Provenance of Wapiti Formation (Eocene) Tuffaceous Sandstones, South Fork Shoshone River Valley, Wyoming: Mountain Geologist, v. 51, p. 279-294.

Malone, D.H., Welch, J.L., Foreman, B., and Craddock, J.P., 2017, Detrital zircon U-Pb geochronology and provenance of the Eocene Willwood Formation, northern Absaroka Basin, Wyoming: The Mountain Geologist, v. 54, p. 104–124, https://doi.org/10.31582/rmag.mg.54.2.104.

Malone, D.H., Craddock, J.P., and Konstantinou, A., 2022, this volume, Timing and structural evolution of the Sevier thrust belt, western Wyoming, *in* Craddock, J.P., Malone, D.H., Foreman, B.Z., and Konstantinou, A., eds., Tectonic Evolution of the Sevier-Laramide Hinterland, Thrust Belt, and Foreland, and Postorogenic Slab Rollback (180–20 Ma): Geological Society of America Special Paper 555, Chapter 4, https://doi.org/10.1130/2022.2555(04).

May, S.R., Gray, G.G., Summa, L.L., Stewart, N.R., Gehrels, G.E., and Pecha, M.E., 2013, Detrital zircon geochronology from the Bighorn Basin, Wyoming, USA: Implications for tectonostratigraphic evolution and paleogeography: Geological Society of America Bulletin, v. 125, no. 9–10, p. 1403–1422, https://doi.org/10.1130/B30824.1.

McCormick, W.L., 1950, A Study of the McDermott Formation, Upper Cretaceous Age in the San Juan Basin, Southwestern Colorado and Northern New Mexico [M.S. thesis]: Urbana, Illinois, University of Illinois, 51 p.

Miall, A.D., 2006, How do we identify big rivers? And how big is big?: Sedimentary Geology, v. 186, p. 39–50, https://doi.org/10.1016/j.sedgeo.2005.10.001.

Miall, A.D., Catuneanu, O., Vakarelov, B.K., and Post, R., 2008, The Western Interior Basin, *in* Miall, A.D., ed., Sedimentary Basins of the World, Volume 5: The Sedimentary Basins of the United States and Canada: Amsterdam, Elsevier, p. 329–362, https://doi.org/10.1016/S1874-5997(08)00009-9.

Miller, D.M., Nilsen, T.H., and Bilodeau, W.L., 1992, Late Cretaceous to early Eocene geologic evolution of the U.S. Cordillera, *in* Burchfiel, B.C., Lipman, P.W., and Zoback, M.L., eds., The Cordilleran Orogen: Conterminous U.S.: Geological Society of America, Geology of North America, v. G-3, p. 205–260, https://doi.org/10.1130/DNAG-GNA-G3.205.

Molenaar, C.M., 1983, Major depositional cycles and regional correlations of Upper Cretaceous rocks, southern Colorado Plateau and adjacent areas, *in* Reynolds, M.W., and Dolly, E.D., eds., Mesozoic Paleogeography of the West-Central United States: Denver, Colorado, Rocky Mountain Section, Society for Sedimentary Geology (SEPM), Paleogeography Symposium 2, p. 201–224.

New Mexico Bureau of Geology and Mineral Resources, 2003, Geologic Map of New Mexico: Socorro, New Mexico, New Mexico Bureau of Geology and Mineral Resources, scale 1:500,000.

O'Shea, C., 2009, Volcanic Influence over Fluvial Sedimentation in the Cretaceous McDermott Member, Animas Formation, Southwestern Colorado [M.S. thesis]: Bowling Green, Kentucky, Bowling Green State University, 90 p.

Pazzaglia, F., and Kelley, S., 1998, Large-scale geomorphology and fission-track thermochronology in topographic and exhumation reconstructions of the southern Rocky Mountains: Rocky Mountain Geology, v. 33, p. 229–257, https://doi.org/10.2113/33.2.229.

Pecha, M.E., Gehrels, G.E., McClelland, W.C., Giesler, D., White, C., and Yokelson, I., 2016, Detrital zircon U-Pb geochronology and Hf isotope geochemistry of the Yukon-Tanana terrane, Coast Mountains, southeast Alaska: Geosphere, v. 12, p. 1556–1574, https://doi.org/10.1130/GES01303.1.

Pecha, M.E., Gehrels, G.E., Karlstrom, K.E., Dickinson, W.R., Donahue, M.S., Gonzales, D.A., and Blum, M.D., 2018, Provenance of Cretaceous through Eocene strata of the Four Corners region: Insights from detrital zircons in the San Juan Basin, New Mexico and Colorado: Geosphere, v. 14, p. 785–811, https://doi.org/10.1130/GES01485.1.

Pederson, J.L., Mackley, R.D., and Eddleman, J.L., 2002, Colorado Plateau uplift and erosion evaluated using GIS: GSA Today, v. 12, p. 4–10, https://doi.org/10.1130/1052-5173(2002)012<0004:CPUAEE>2.0.CO;2.

Poag, C.W., and Sevon, W.D., 1989, A record of Appalachian denudation in postrift Mesozoic and Cenozoic sedimentary deposits of the U.S. Middle Atlantic continental margin: Geomorphology, v. 2, p. 119–157, https://doi.org/10.1016/0169-555X(89)90009-3.

Potter-McIntire, S.L., Breeden, J.R., and Malone, D.H., 2018, A Maastrichtian birth of the Mississippi River: Cretaceous Research, v. 91, p. 71–78, https://doi.org/10.1016/j.cretres.2018.05.010.

Powell, J.S., 1972, The Gallegos Sandstone (formerly Ojo Alamo Sandstone) of the San Juan Basin, New Mexico [M.S. thesis]: Tucson, Arizona, University of Arizona, 131 p.

Pullen, A., Ibanez-Mejia, M., Gehrels, G., Giesler, D., and Pecha, M., 2018, Optimization of a laser ablation–single collector–inductively coupled plasma–mass spectrometer (Thermo Element 2) for accurate, precise, and efficient zircon U-Th-Pb geochronology: Geochemistry, Geophysics, Geosystems, v. 19, no. 10, p. 3689–3705, https://doi.org/10.1029/2018GC007889.

Reeside, J.B., Jr., 1924, Upper Cretaceous and Tertiary Formations of the Western Part of the San Juan Basin, Colorado and New Mexico: U.S. Geological Survey Professional Paper 134, 70 p., https://doi.org/10.3133/pp134.

Saleeby, J.B., 2003, Segmentation of the Laramide slab—Evidence from the southern Sierra Nevada region: Geological Society of America Bulletin, v. 115, p. 655–668, https://doi.org/10.1130/0016-7606(2003)115<0655:SOTLSF>2.0.CO;2.

Sauer, K.B., Gordon, S.M., Miller, R.B., Vervoort, J.D., and Fisher, C.M., 2017, Evolution of the Jura-Cretaceous North American Cordilleran margin: Insights from detrital-zircon U-Pb and Hf isotopes of sedimentary units of the North Cascades Range, Washington: Geosphere, v. 13, p. 2094–2118, https://doi.org/10.1130/GES01501.1.

Schwartz, T.M., and Schwartz, R.K., 2013, Paleogene postcompressional intermontane basin evolution along the frontal Cordilleran fold-and-thrust

belt of southwestern Montana: Geological Society of America Bulletin, v. 125, p. 961–984, https://doi.org/10.1130/B30766.1.

Schwartz, T.M., Methner, K., Mulch, A., Graham, S.A., and Chamberlain, C.P., 2019, Paleogene topographic and climatic evolution of the northern Rocky Mountains from integrated sedimentary and isotopic data: Geological Society of America Bulletin, v. 131, p. 1203–1223, https://doi.org/10.1130/B32068.1.

Sewall, J.O., and Sloan, L.C., 2006, Come a little bit closer: A high-resolution climate study of the early Paleogene Laramide foreland: Geology, v. 34, p. 81–84, https://doi.org/10.1130/G22177.1.

Sharman, G.R., Graham, S.A., Grove, M., Kimbrough, D.L., and Wright, J.E., 2015, Detrital zircon provenance of the Late Cretaceous–Eocene California forearc: Influence of Laramide low-angle subduction on sediment dispersal and paleogeography: Geological Society of America Bulletin, v. 127, p. 38–60, https://doi.org/10.1130/B31065.1.

Sharman, G.R., Covault, J.A., Stockli, D.F., Wroblewski, A.F.-J., and Bush, M.A., 2017, Early Cenozoic drainage reorganization of the United States Western Interior–Gulf of Mexico sediment routing system: Geology, v. 45, p. 187–190, https://doi.org/10.1130/G38765.1.

Sharman, G.R., Stockli, D.F., Flaig, P., Raynolds, R.G., Dechesne, M., and Covault, J.A., 2022, this volume, Tectonic influence on axial-transverse sediment routing in the Denver Basin, *in* Craddock, J.P., Malone, D.H., Foreman, B.Z., and Konstantinou, A., eds., Tectonic Evolution of the Sevier-Laramide Hinterland, Thrust Belt, and Foreland, and Postorogenic Slab Rollback (180–20 Ma): Geological Society of America Special Paper 555, Chapter 11, https://doi.org/10.1130/2021.2555(11).

Shaw, S.E., Todd, V.R., Kimbrough, D.L., and Pearson, N.J., 2014, A west-to-east geologic transect across the Peninsular Ranges batholith, San Diego County, California: Zircon $^{176}Hf/^{177}Hf$ evidence for the mixing of crustal- and mantle-derived magmas, and comparisons with the Sierra Nevada batholith, *in* Morton, D.M., and Miller, F.K., eds., Peninsular Ranges Batholith, Baja California and Southern California: Geological Society of America Memoir 211, p. 499–536, https://doi.org/10.1130/2014.1211(15).

Sikkink, P.G.L., 1987, Lithofacies relationships and depositional environment of the Tertiary Ojo Alamo Sandstone and related strata, San Juan Basin, New Mexico and Colorado, *in* Fassett, J.E., and Rigby, J.K., Jr., eds., The Cretaceous-Tertiary Boundary in the San Juan and Raton Basins, New Mexico and Colorado: Geological Society of America Special Paper 209, p. 81–104, https://doi.org/10.1130/SPE209-p81.

Sklar, L.S., and Dietrich, W.E., 2001, Sediment and rock strength controls on river incision into bedrock: Geology, v. 29, p. 1087–1090, https://doi.org/10.1130/0091-7613(2001)029<1087:SARSCO>2.0.CO;2.

Slattery, J.S., Cobban, W.A., McKinney, K.C., Harries, P.J., and Sandness, A.L., 2015, Early Cretaceous to Paleocene paleogeography of the Western Interior Seaway: The interaction of eustasy and tectonism, *in* Bingle-Davis, M., ed., 68th Annual Field Conference Guidebook: Casper, Wyoming, Wyoming Geological Association, p. 22–60.

Smith, L.N., 1988, Basin Analysis of the Lower Eocene San Jose Formation, San Juan Basin, New Mexico and Colorado [Ph.D. dissertation]: Albuquerque, New Mexico, University of New Mexico, 166 p.

Smith, M.E., Carroll, A.R., Jicha, B.R., Cassel, E.J., and Scott, J.J., 2014, Paleogeographic record of Eocene Farallon slab rollback beneath western North America: Geology, v. 42, p. 1039–1042, https://doi.org/10.1130/G36025.1.

Smith, T.M., Sundell, K.E., Johnston, S., Guilherme Andrade, C., Andrea, R., Dickinson, J., Liu, Y., Murphy, M.A., Lapen, T.J., and Saylor, J.E., 2020, Drainage reorganization and Laramide tectonics in north-central New Mexico and their downstream effects in the Gulf of Mexico: Basin Research, v. 32, no. 3, p. 419–452, https://doi.org/10.1111/bre.12373.

Snedden, J.W., Galloway, W.E., Milliken, K.T., Xu, J., Whitaker, T., and Blum, M.D., 2018, Validation of empirical source to sink scaling relationships in a continental scale system: The Gulf of Mexico Basin Cenozoic record: Geosphere, v. 14, no. 2, p. 768–784, https://doi.org/10.1130/GES01452.1.

Sømme, T.O., Helland-Hansen, W., and Granjeon, D., 2009, Impact of eustatic amplitude variations on shelf morphology, sediment dispersal, and sequence stratigraphic interpretation: Icehouse versus greenhouse systems: Geology, v. 37, p. 587–590, https://doi.org/10.1130/G25511A.1.

Sundell, K.E., Saylor, J.E., and Pecha, M., 2019, Sediment provenance and recycling of detrital zircons from Cenozoic Altiplano strata in southern Peru and implications for crustal evolution of west-central South America, *in* Horton, B.K., and Folguera, A., eds., Andean Tectonics: Amsterdam, Elsevier, p. 363–397, https://doi.org/10.1016/B978-0-12-816009-1.00014-9.

Surpless, K.D., and Gulliver, K.D.H., 2018, Provenance analysis of the Ochoco basin, central Oregon: A window into the Late Cretaceous paleogeography of the northern U.S. Cordillera, *in* Ingersoll, R.V., Graham, S.A., and Lawton, T.F., eds., Tectonics, Sedimentary Basins, and Provenance: A Celebration of William R. Dickinson's Career: Geological Society of America Special Paper 540, p. 235–266, https://doi.org/10.1130/2018.2540(11).

Surpless, K.D., Sickmann, Z.T., and Koplitz, T.A., 2014, East-derived strata in the Methow basin record rapid mid-Cretaceous uplift of the southern Coast Mountains batholith: Canadian Journal of Earth Sciences, v. 42, p. 1163–1185, https://doi.org/10.1139/e04-086.

Tribe, S, 2005, Eocene paleo-physiography and drainage directions, southern Interior Plateau, British Columbia: Canadian Journal of Earth Sciences, v. 42, p. 215–230, https://doi.org/10.1139/e04-062.

Vervoort, J.D., and Blichert-Toft, J., 1999, Evolution of the depleted mantle: Hf isotope evidence from juvenile rocks through time: Geochimica et Cosmochimica Acta, v. 63, p. 533–556, https://doi.org/10.1016/S0016-7037(98)00274-9.

Vervoort, J.D., and Patchett, P.J., 1996, Behavior of hafnium and neodymium isotopes in the crust: Constraints from crustally derived granites: Geochimica et Cosmochimica Acta, v. 60, p. 3717–3733, https://doi.org/10.1016/0016-7037(96)00201-3.

Vervoort, J.D., Patchett, P.J., Blichert-Toft, J., and Albarède, F., 1999, Relationships between Lu-Hf and Sm-Nd isotopic systems in the global sedimentary system: Earth and Planetary Science Letters, v. 168, p. 79–99, https://doi.org/10.1016/S0012-821X(99)00047-3.

Wahl, P.J., Yancey, T.E., Pope, M.C., Miller, B.V., and Ayers, W.B., 2016, U-Pb detrital zircon geochronology of the Upper Paleocene to Lower Eocene Wilcox Group, east-central Texas: Geosphere, v. 12, p. 1517–1531, https://doi.org/10.1130/GES01313.1.

Walker, J.D., and Geissman, J.W., 2009, 2009 GSA geologic time scale: GSA Today, v. 19, no. 4–5, p. 60–61, https://doi.org/10.1130/1052-5173-19.4-5.60.

Welch, J.L., Foreman, B.Z., Malone, D., and Craddock, J., 2022, this volume, Provenance of early Paleogene strata in the Bighorn Basin (Wyoming, USA): Implications for Laramide tectonism and basin-scale stratigraphic patterns, *in* Craddock, J.P., Malone, D.H., Foreman, B.Z., and Konstantinou, A., eds., Tectonic Evolution of the Sevier-Laramide Hinterland, Thrust Belt, and Foreland, and Postorogenic Slab Rollback (180–20 Ma): Geological Society of America Special Paper 555, Chapter 9, https://doi.org/10.1130/2022.2555(09).

White, C., Gehrels, G., Pecha, M., Giesler, D., Yokelson, I., McClelland, W., and Butler, R., 2016, U-Pb and Hf isotope analysis of detrital zircons from Paleozoic strata of the southern Alexander terrane (southeast Alaska): Lithosphere, v. 8, p. 83–96, https://doi.org/10.1130/L475.1.

Whitmeyer, S.J., and Karlstrom, K.E., 2007, Tectonic model for the Proterozoic growth of North America: Geosphere, v. 3, p. 220–259, https://doi.org/10.1130/GES00055.1.

Wilf, P., 2000, Late Paleocene–early Eocene climate changes in southwestern Wyoming: Paleobotanical analysis: Geological Society of America Bulletin, v. 112, p. 292–307, https://doi.org/10.1130/0016-7606(2000)112<292:LPECCI>2.0.CO;2.

Wyld, A.J., Umhoefer, P.J., and Wright, J.E., 2006, Reconstructing northern Cordilleran terranes along known Cretaceous and Cenozoic strike-slip faults: Implications for the Baja British Columbia hypothesis and other models, *in* Haggart, J.W., Enkin, R.J., and Monger, J.W.H., eds., Paleogeography of the North American Cordillera: Evidence For and Against Large-Scale Displacements: Geological Association of Canada Special Paper 46, p. 277–298.

Yokelson, I., Gehrels, G., Pecha, M., Giesler, D., White, C., and McClelland, W., 2015, U-Pb and Hf isotope analysis of detrital zircons from Mesozoic strata of the Gravina belt, southeast Alaska: Tectonics, v. 34, p. 2052–2066, https://doi.org/10.1002/2015TC003955.

Zarra, L., Hackworth, R., and Kahn, A., 2019, Wilcox chronostratigraphic framework update: American Association of Petroleum Geologists (AAPG) Search and Discovery Article 51616 (adapted from extended abstract based on poster presentation given at AAPG Annual Convention & Exhibition, San Antonio, Texas, 19–22 May 2019), https://www.searchanddiscovery.com/pdfz/documents/2019/51616zarra/ndx_zarra.pdf.html.

Manuscript Accepted by the Society 16 August 2021
Manuscript Published Online 29 March 2022
Printed in the USA